JGR Space Physics

RESEARCH ARTICLE
10.1029/2018JA026066

Special Section:
Particle Dynamics in the Earth's Radiation Belts

The Response of Earth's Electron Radiation Belts to Geomagnetic Storms: Statistics From the Van Allen Probes Era Including Effects From Different Storm Drivers

D. L. Turner[1], E. K. J. Kilpua[2], H. Hietala[3,4], S. G. Claudepierre[1], T. P. O'Brien[1], J. F. Fennell[1], J. B. Blake[1], A. N. Jaynes[5], S. Kanekal[6], D. N. Baker[7], H. E. Spence[8], J.-F. Ripoll[9], and G. D. Reeves[10]

[1]Space Sciences Department, The Aerospace Corporation, El Segundo, CA, USA, [2]Department of Physics, University of Helsinki, Helsinki, Finland, [3]Department of Earth, Planetary, and Space Sciences, University of California, Los Angeles, CA, USA, [4]Department of Physics and Astronomy, University of Turku, Turku, Finland, [5]Department of Physics and Astronomy, University of Iowa, Iowa City, IA, USA, [6]NASA Goddard Space Flight Center, Greenbelt, MD, USA, [7]Laboratory for Atmospheric and Space Physics, University of Colorado Boulder, Boulder, CO, USA, [8]Institute For the Study of Earth, Oceans, and Space, University of New Hampshire, Durham, NH, USA, [9]CEA, DAM, DIF, Arpajon, France, [10]Los Alamos National Laboratory, Los Alamos, NM, USA

Key Points:
- A statistical model of electron radiation belt response to storms as a function of energy and L-shell is developed
- Storm-time morphology of the electron radiation belts is qualitatively predictable
- Results are better organized when the solar wind drivers of storms are identified

Supporting Information:
- Supporting Information S1

Correspondence to:
D. L. Turner,
drew.l.turner@aero.org

Citation:
Turner, D. L., Kilpua, E. K. J., Hietala, H., Claudepierre, S. G., O'Brien, T. P., Fennell, J. F., et al. (2019). The response of Earth's electron radiation belts to geomagnetic storms: Statistics from the Van Allen Probes era including effects from different storm drivers. *Journal of Geophysical Research: Space Physics*, *124*, 1013–1034. https://doi.org/10.1029/2018JA026066

Received 5 SEP 2018
Accepted 4 JAN 2019
Accepted article online 11 JAN 2019
Published online 13 FEB 2019

Abstract A statistical study was conducted of Earth's radiation belt electron response to geomagnetic storms using NASA's Van Allen Probes mission. Data for electrons with energies ranging from 30 keV to 6.3 MeV were included and examined as a function of L-shell, energy, and epoch time during 110 storms with *SYM-H* ≤−50 nT during September 2012 to September 2017 (inclusive). The radiation belt response revealed clear energy and L-shell dependencies, with tens of keV electrons enhanced at all L-shells ($2.5 \le L \le 6$) in all storms during the storm commencement and main phase and then quickly decaying away during the early recovery phase, low hundreds of keV electrons enhanced at lower L-shells ($\sim 3 \le L \le \sim 4$) in upward of 90% of all storms and then decaying gradually during the recovery phase, and relativistic electrons throughout the outer belt showing main phase dropouts with subsequent and generally unpredictable levels of replenishment during the recovery phase. Compared to prestorm levels, electrons with energies >1 MeV also revealed a marked increase in likelihood of a depletion at all L-shells through the outer belt ($3.5 \le L \le 6$). Additional statistics were compiled revealing the storm time morphology of the radiation belts, confirming the aforementioned qualitative behavior. Considering storm drivers in the solar wind: storms driven by coronal mass ejection (CME) shocks/sheaths and CME ejecta only are most likely to result in a depletion of >1-MeV electrons throughout the outer belt, while storms driven by full CMEs and stream interaction regions are most likely to produce an enhancement of MeV electrons at lower ($L < \sim 5$) and higher ($L > \sim 4.5$) L-shells, respectively. CME sheaths intriguingly result in a distinct enhancement of ~1-MeV electrons around L~5.5, and on average, CME sheaths and stream interaction regions result in double outer belt structures.

1. Introduction

Earth's magnetosphere operates as a highly efficient particle accelerator that is responsible for producing the very high intensities of relativistic electrons that constitute the Van Allen radiation belts in near-Earth space. It has long been known (e.g., Dessler & Karplus, 1961) that the electron radiation belts are a highly dynamic region, with intensities of relativistic electrons in the outer belt and slot region often fluctuating by multiple orders of magnitude over time scales as short as a few hours (e.g., Friedel et al., 2002; Li et al., 1999; Millan & Thorne, 2007; Reeves et al., 1998; Reeves et al., 2013; Thorne, Li, Ni, Ma, Bortnik, Baker, et al., 2013; Thorne, Li, Ni, Ma, Bortnik, Chen, et al., 2013; Turner et al., 2012). In addition to being of scientific interest, it is also of practical importance to understand radiation belt variability and its underlying drivers, since outer radiation belt electrons pose a threat to both crewed and uncrewed space missions.

Electron radiation belt variability is particularly evident during geomagnetic storms (e.g., Baker, Jaynes, Turner, et al., 2016; Baker, Jaynes, Kanekal, et al., 2016), which is the focus of this statistical study.

Geomagnetic storms are several day periods of intensified magnetospheric activity distinguished particularly by the perturbations to ground-based measurements of Earth's intrinsic magnetic field associated with an enhanced ring current in near-Earth space (e.g., Gonzalez et al., 1994). Storm activity is broken into different phases based on the *Dst* or *SYM-H* geomagnetic indices that are determined from low- to middle-latitude magnetometer stations, thus reflecting changes in the ring current intensity. Storm sudden commencement is defined as a positive perturbation of *SYM-H* or *Dst* associated with a compression of the magnetosphere from some enhancement in the solar wind pressure that is then followed by a geomagnetic storm. The main phase of the storm is characterized by ring current intensification resulting in a strong negative perturbation to *SYM-H* or *Dst*, with the peak of the main phase being the point of *Dst* or *SYM-H* minimum. Storm intensities range from *SYM-H* minima ≤ -30 nT to minima < -300 nT, with there being no lower limit on the intensity (the more negative the *SYM-H*, or *Dst*, the stronger the geomagnetic disturbance). For most storms, the sudden commencement and main phase last approximately one day or less. After the peak of the main phase, the ring current returns to its typical state and *Dst* and *SYM-H* return to average, nonstorm levels during a period known as the recovery phase of the storm, which usually lasts several days. Some references for more details on geomagnetic storms include Kamide et al. (1998), Gonzalez et al. (1999), Hutchinson et al. (2011), and Katus et al. (2011).

Many previous studies have also been devoted to understanding the outer electron radiation belt's response to geomagnetic storms. O'Brien et al. (2001) conducted a statistical study of the outer belt storm response using 0.3- to >2-MeV electron data from NOAA's GOES and Los Alamos National Laboratory (LANL) spacecraft at geosynchronous orbit (GEO). They conducted cross-correlation analysis of solar wind and geomagnetic activity data for 33 storms that caused an enhancement of electrons at GEO and 29 storms that did not. They found that main phase intensity, as defined by geomagnetic indices, is not a good indicator of the electron response at GEO but also that storm duration, sustained and above-average solar wind speed, elevated Pc5 ultralow-frequency (ULF) wave power in the magnetosphere, and sustained, enhanced substorm activity indicated by the auroral electrojet (*AE*) index during the recovery phase were the best indicators of those storms that result in an enhancement of electrons at GEO. Reeves et al. (2003) conducted a study of 276 moderate to intense storms ($Dst < -50$ nT) and the outer belt response using 1.8–3.5-MeV electrons observed by the LANL-GEO spacecraft. They found that 53% of storms caused an enhancement of relativistic electrons at GEO, 19% caused a depletion at GEO, and 28% caused no significant change (within a factor of 2). They concluded that the somewhat unpredictable nature of the outer belt response to storms was the results of a "delicate and complicated balance between the effects of particle acceleration and loss" (Reeves et al., 2003, pp. 36–1). Anderson et al. (2015) conducted a similar study, but instead examined small storms with $Dst > -50$ nT. They collected data from 342 small storms from 1989 to 2000, and found that small storms are 10% less (more) likely to result in a flux enhancement (depletion) at GEO compared to large storms. Turner, O'Brien, et al. (2015) and Moya et al. (2017) closely followed the Reeves et al. (2003) study but used tens of keV to multi-MeV electron observations from throughout the outer belt observed by NASA's Van Allen Probes mission. Turner, O'Brien, et al. (2015) found that several hundreds of keV electrons were enhanced at L-shells of 3 to 4 in upward of 90% of storms, while both Turner, O'Brien, et al. (2015) and Moya et al. (2017) found that the results for MeV electrons were more unpredictable, essentially generalizing the Reeves et al. (2003) results to the rest of the outer belt.

Using data from NOAA's POES spacecraft in highly inclined low-Earth orbit (LEO), Horne et al. (2009) assembled statistics from 69 geomagnetic storms with $Dst \leq -70$ nT during 1998 to 2007. They found that the atmospheric precipitation of >300-keV electrons peaks during the main phase of storms, while that of >1-Mev electrons peaks in the recovery phase, and that wave-particle interactions are evidently sufficient to scatter >300-keV electrons directly into the bounce loss cone but only capable of scattering >1-MeV electrons into the drift loss cone. Zhao and Li (2013) also studied the statistical response of the radiation belt electrons during storms at LEO using SAMPEX observations; from 119 storms, they found that 2–6-MeV electrons penetration depth in L-shell, maximum flux level, and maximum flux variation all had strong correlation with minimum *Dst*. They also recorded 23 cases with injections of 2–6-MeV electrons into $L = 2.5$.

Murphy et al. (2018) conducted a statistical study using total radiation belt content derived from Van Allen Probes data. They described two phases: one during the main phase dominated by loss followed by another during the recovery phase dominated by acceleration. Since the study used phase space density for constant values of electron first adiabatic invariants, the analysis effectively removed any adiabatic variations that

might obfuscate results compiled using flux as a function of energy. Thus, the phases of loss and acceleration/source clearly distinguished two distinct periods of outer radiation belt behavior during geomagnetic storms. Concerning acceleration and active sources of relativistic electrons, Kim et al. (2015) examined 65 geomagnetic storms and 17 nonstorm relativistic electron enhancement events at GEO and found that enhancement events can occur independently of storm activity. Similarly, Li et al. (2015), Zhao et al. (2017), and Pinto et al. (2018) all conducted statistical studies of enhancement events regardless of storm activity. All of these studies (plus many others) agree that conditions such as solar wind velocity enhancements, interplanetary magnetic field (IMF), southward (i.e., negative) B_z, sustained substorm activity, and enhanced ULF and VLF wave power are all correlated with enhancements of relativistic electrons in the outer radiation belt.

Several statistical studies have also investigated the roles of different storm drivers in the solar wind (e.g., Kilpua et al., 2017), that is, the distinguishable solar wind characteristics that result in a geomagnetic storm. These studies all found that distinguishing by different solar wind storm drivers helps when determining the effect a particular storm will have on radiation belt electrons. Hudson et al. (2008) present a review on the relationship between radiation belt electrons and different solar wind drivers. Borovsky and Denton (2006) compared and contrasted the differences between storms driven by coronal mass ejections (CMEs) versus those driven by corotating interaction regions (CIRs; a.k.a., stream interaction regions, SIRs, where high-speed streams, HSS, overtake the slower solar wind ahead of them forming a compression region where the slow and fast streams are separated by a stream interface); for radiation belt responses, quantified using data from GEO, they found that CIR-driven storms result in more severe enhancements of outer belt electrons at GEO compared to CME-driven storms. Kataoka and Miyoshi (2006) conducted a similar study using >2-MeV electron data from GEO and found that the response to CME-driven storms was mixed while the majority of CIR-driven storms resulted in enhancements of >2-MeV electrons at GEO during the first several days of the storm recovery phase. Morley et al. (2010) studied the dropout response of relativistic electrons to SIR events observed over a range of L-shells in the outer belt by the Global Positioning System satellites, and found that the dropout and subsequent redevelopment of the outer belt electrons was strongly dependent on L-shell. Yuan and Zong (2012) examined data from 54 CME-driven storms and 26 CIR-driven storms with relativistic electron data from SAMPEX at LEO. They found that for electrons summed over all L-shells in the outer belt (at LEO), CME storms resulted in larger enhancements of outer belt electrons compared to CIR storms, but CIR storms produced larger enhancements at L-shells corresponding to GEO. Shen et al. (2017) also compared and contrasted 28 CME-driven versus 31 CIR-driven storms using Van Allen Probes data at three L-shell ranges in the outer belt; they found notable differences, including that CMEs drive enhancements of electrons that are most intense at lower L-shells compared to enhancements in CIR storms. Yuan and Zong (2013) studied the outer belt response to over 300 CME- and CIR-driven storms using SAMPEX data, found that eight of the events resulted in clear double-outer-belt structures (i.e., two peaks in the radial profiles of relativistic electrons), and concluded that the plasmapause plays an important role in the development and evolution of double outer belt structures. Most recently, Benacquista et al. (2018) examined the statistical response of electrons over four energy ranges (>30, >100, >300 keV, and >1 MeV) from NOAA-POES satellites in LEO during storms driven by CMEs and CIRs; they too found that the effect of storms on the outer belt electrons were both L-shell and driver dependent.

Meredith et al. (2011) looked at electron precipitation from the outer radiation belt in response to HSS-driven storms using NOAA POES data at LEO. They found that the precipitation of MeV electrons actually decreased during the storm sudden commencement and main phase and then subsequently increased during the recovery phase to levels that exceeded the prestorm average. Miyoshi et al. (2013) separated 216 HSS events between those with predominantly northward versus southward IMF, and they found that southward IMF was also a necessary condition for radiation belt enhancements at GEO. Borovsky et al. (2016) studied two solar cycles worth of HSS-driven storms using LANL-GEO data from 1976 to 1995. They found that the electron radiation belts can be enhanced in such storms directly by a single substorm that occurs during the prolonged recovery phase associated with HSS-driven (a.k.a., CIR-driven) storms; they also reported injections of protons and electrons up to 1 MeV during such substorms.

Hietala et al. (2014) delved further into the outer electron radiation belt's response to CME-driven storms, examining the response of the outer belt electrons to CME sheaths (see also Kilpua et al., 2017). From a statistical study of GOES >2-MeV electron data from 31 storms driven by CME sheaths, they found that such

events tend to result in strong depletions of the radiation belt electrons at GEO. They concluded that CME sheaths have ideal conditions for driving strong losses of electrons to the magnetopause via magnetopause incursions and the *Dst* effect (i.e., collectively known as "magnetopause shadowing") and enhanced outward radial transport driven by ULF waves. Kilpua et al. (2015) followed this study by examining statistics from 193 isolated geomagnetic storms, again using >2-MeV electrons from GOES at GEO. They divided the storms into four subsets, events driven by (1) CME-shock/sheath only, (2) CME-ejecta only, (3) full CMEs (shock/sheath + ejecta), and (4) SIRs. In addition to confirming the results from Hietala et al. (2014) for CME-shock/sheath events, they also found that storms driven by CIRs, full CMEs, and CME ejecta with fast solar wind (>500 km/s for a prolonged period of the recovery phase) during the recovery phases typically resulted in enhancements of relativistic electrons at GEO compared to prestorm levels. CME ejecta and full CMEs with slow solar wind during the recovery phases typically resulted in depletions compared to prestorm levels.

In this study we continue to develop the picture of how Earth's radiation belt electrons respond to geomagnetic storms. This study is intended to expand the statistics of storm time responses of radiation belt electrons throughout the slot and outer radiation belt using the excellent energy and temporal resolution afforded by NASA's Van Allen Probes. In particular, we expand upon previous studies by investigating the energy- and L-shell-dependent structure of the radiation belt electrons and how those structures evolve during geomagnetic storms that are driven by different types of solar wind events. This paper is structured as follows. Section 2 describes the data and methods used for this study. Section 3 details the results, while section 4 provides a discussion of their relevance and context considering previous work. Suggestions for future studies are also offered in section 4. Section 5 delivers a summary and the conclusions derived from this study.

2. Data and Methods

This paper follows closely after the methodology described in Turner, O'Brien, et al. (2015). The primary data sets employed for this study are from NASA's Van Allen Probes mission (Mauk et al., 2013) and the OMNI data set of solar wind quantities propagated to Earth's location plus geomagnetic indices. To identify geomagnetic storms, we used the *SYM-H* index and searched for storm main phases characterized by localized minima satisfying $SYM\text{-}H \leq -50$ nT. For each storm, epoch time zero is set to the universal time at *SYM-H* minimum. To avoid muddling results by combining storms, any events with two such minima within two days of each other were further scrutinized: for so-called "double-dip" storms, with two distinct minima during the storm main phase (e.g., 08–09 October 2012), these storms are included with the epoch time selected as the time of the stronger *SYM-H* minima. However, two distinct storms, where the second event clearly occurs during the recovery phase of the first event (e.g., on 07–11 November 2013), were excluded from this study. These selection criteria resulted in 110 geomagnetic storms identified between September 2012 and September 2017; the epoch times and corresponding *SYM-H* minima for those events are listed in Appendix A. Additional solar wind and geomagnetic index data from the OMNI data set used for this study included solar wind velocity (i.e., the components and magnitude); dynamic pressure, density, temperature, plasma beta, and Mach number; the IMF vector and strength; solar wind V_xB_z-south (X component of the velocity vector multiplied by the southward B_z component of the IMF, a proxy for enhanced magnetospheric reconnection and convection); and the *SYM-H*, PCN, *AL*, *AU*, *AE*, *AL**, and *AE** indices (at any time, *AL** and *AE** are the minimum and maximum of the *AL* and *AE* indices, respectively, over the previous 3 hr).

Van Allen Probes data from the RBSP-ECT instrument suite (Spence et al., 2013) were used to characterize the storm time response of electrons in the radiation belts. More specifically, omnidirectional-averaged electron data from the Magnetic Electron and Ion Spectrometer (MagEIS; Blake et al., 2013) and the Relativistic Electron and Proton Telescope (REPT; Baker, Kanekal, Hoxie, Batiste, et al., 2013; Baker, Kanekal, Hoxie, Henderson, et al., 2013) instruments on both spacecraft were employed. For this study, we used background-corrected MagEIS data (Claudepierre et al., 2015; Claudepierre et al., 2017). Both MagEIS and REPT data are available at 11-s temporal resolution and were binned for this study in epoch time ($\Delta t = 6$ hr) and L-shell ($\Delta L = 0.1$) during each of the 110 storms identified. Here we limit our study to $2.5 \leq L \leq 6.0$ to account for REPT contamination in the inner radiation belt and the apogees of the Van Allen Probes' orbits. The Van Allen Probes take ~4.5 hr to cross from perigee to apogee and across all of the L-shells used here, ensuring dozens of data points in each storm's time-L bins at L = 2.5 and up to

thousands at L = 6.0. For this study, we used MagEIS data covering electron energies from 32 keV up to 1.5 MeV and REPT data covering energies from 1.8 to 6.3 MeV. Following Reeves et al. (2003) and Turner, O'Brien, et al. (2015), we excluded ±12-hr epoch time and used a factor of 2x change for the prestorm and poststorm characterization of enhancement, depletion, or no change. To qualify as an enhancement (depletion), the poststorm maximum flux from 12- to 84-hr epoch time at a particular energy and L-shell must increase (decrease) by a factor of 2x above (below) the prestorm maximum flux from −84- to −12-hr epoch time. Again, please refer to Turner, O'Brien, et al. (2015) for additional details on the data handling, as we have followed that methodology. We also recalculated the results using a factor of 5x instead, which resulted in more "no change" events but overall did not affect the key features of the distributions that we focus on here. Expanding upon the Turner, O'Brien, et al. (2015) study here, we included more storms and REPT data and performed a much more comprehensive statistical analysis with the results.

With data from 24 energy channels spanning 30 keV to 6.3 MeV binned in L-shell and epoch time, the statistical response of electrons throughout the radiation belts was compiled for the full set and different subsets of the 110 storms (e.g., Moya et al., 2017; Turner, O'Brien, et al., 2015). In the next section, we discuss the results from all 110 storms plus subsets of storms distinguished by the storm-driver in the solar wind.

3. Results

3.1. Solar Wind and Geomagnetic Indices

Solar wind and geomagnetic index data from all 110 storms plus statistical quantities are shown in Figure 1, which shows data from all storms with the charcoal gray lines plus means, medians, quartiles, and 5 and 95% confidence intervals in red, blue, turquoise, and green, respectively. Such statistics have been presented for storms before (O'Brien et al., 2001), and the results in Figure 1 are generally consistent. Data are plotted versus epoch time, and by definition of the event selection criteria, all of the storms had *SYM-H* ≤ −50 nT at 0-hr epoch time. The *AE* index, an indicator of substorm activity, peaks just before 0-hr epoch time, during the main phase of the storms, and the distribution of *AE* indices is essentially lognormal (i.e., the spread in the distribution indicated by the separation between the median and the 5 and 95% confidence intervals is approximately a constant multiplicative factor). In some storms, *AE* stays elevated throughout most of the recovery phase, while in others it is only really elevated during the main phase, which might play a key role in whether or not the storm is effective at enhancing the outer radiation belt (e.g., Meredith et al., 2002). IMF B_z is southward (i.e., negative) in ~95% of storm main phases, when energy transfer from the solar wind to the magnetosphere (indicated with V_xB_zs) is also strongest. Solar wind dynamic pressure is enhanced in the day and a half leading up to *SYM-H* minima, while solar wind speed is enhanced on average during the main and recovery phases of storms. These are important points to raise concerning the effects on Earth's radiation belt electrons.

3.2. Storm Time Morphology of Radiation Belt Electrons: All Events

Following Reeves et al. (2003), Turner, O'Brien, et al. (2015), and Moya et al. (2017), Figure 2 shows the percentage of electron radiation belt enhancement events, depletion events, and no-change events as a function of L-shell and energy from these 110 storms. Consistent with Reeves et al. (2003) results at GEO, approximately half (47%) of the events show an enhancement of 1.8-MeV electrons at L = 6, while the other half show either a depletion (31%) or no change (22%) from prestorm levels. Consistent with the results of Turner, O'Brien, et al. (2015), geomagnetic storms tend to result in an enhancement of hundreds of keV electrons at 3 ≤ L ≤ 4.5 in the majority (>75%) of storms. Consistent with the results of Moya et al. (2017), MeV electrons have an ~30 to 50% likelihood to be enhanced at L-shells >4, yet depletions are also likely (~30 to 45%) to occur for MeV electrons over a broad range of L > ~3.5. At L-shells throughout the outer radiation belt, there is a distinct jump in likelihood of depletions for electrons with energies >~1.5 MeV. No-change events are most common for tens to hundreds of keV electrons at L ≤ 3.5 because of the stability of the inner radiation belt, while at higher L-shells (L > ~5), substorm injections replenish those electrons during the main and recovery phases, resulting in no change or enhancements being common there. For relativistic electrons, >500 keV, no-change events are most common at 2.5 ≤ L < 3.5 because of the slot region; essentially, the population there remains nonexistent from prestorm to poststorm in the majority of events. The same is true for the prevalence of no-change events for ≥5-MeV electrons at higher L-shells.

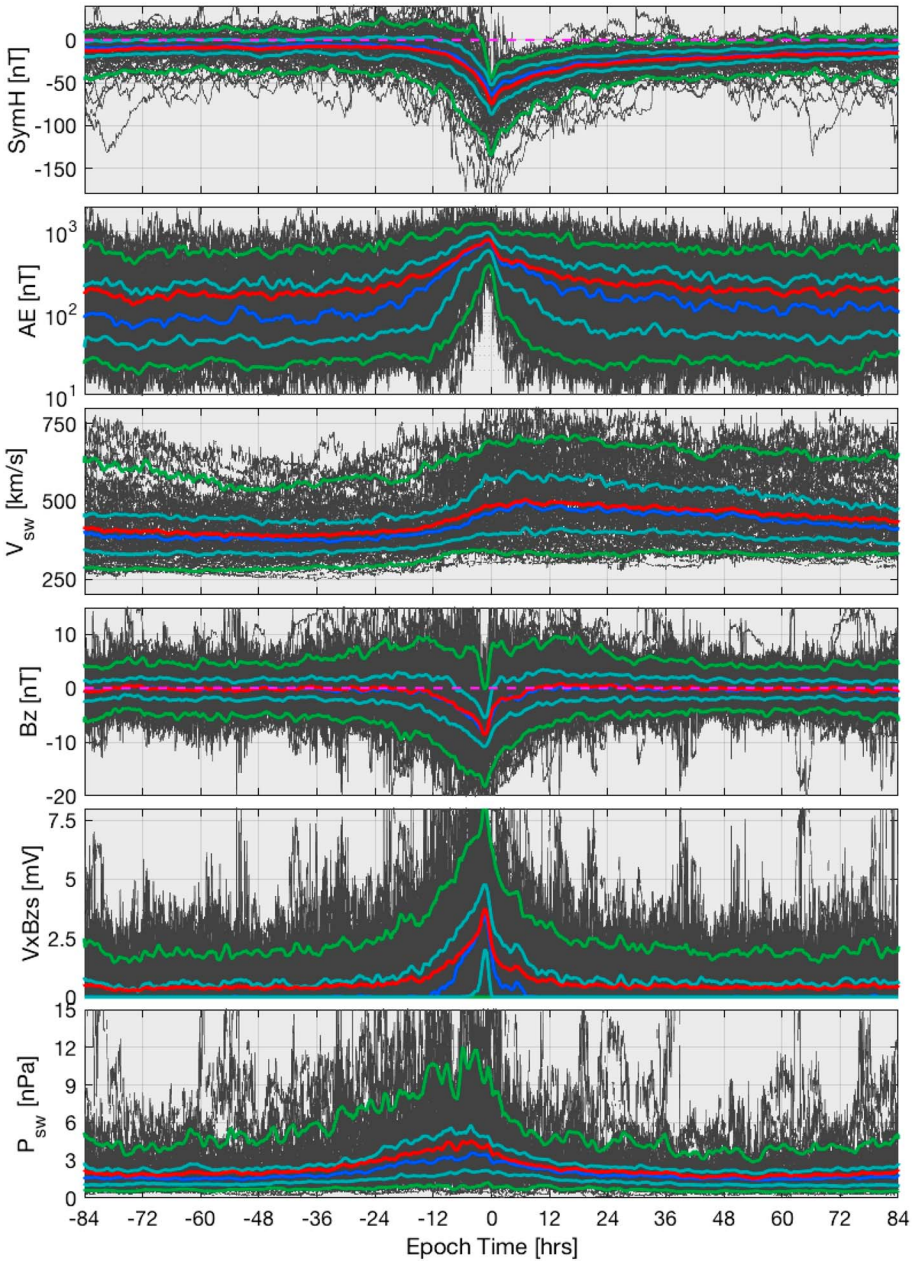

Figure 1. Superposed epoch analysis results of OMNI solar wind and geomagnetic index data. For all panels, data from all storms are shown plotted versus epoch hour in charcoal gray. Statistics from these data are shown as follows: means in red, medians in blue, upper and lower quartiles in turquoise, and 5% and 95% confidence intervals in green. Panels from top to bottom show *SYM-H* index, *AE* index, solar wind speed (V_{sw}), IMF B_z, solar wind V_x multiplied by the southward component of IMF B_z (i.e., this quantity is zero when $B_z \geq 0$ nT), and solar wind dynamic pressure (P_{sw}).

Another way to examine the distribution of responses of Earth's radiation belt electrons to geomagnetic storms is to examine statistical quantities of electron flux as a function of epoch time, L-shell, and energy. Figure 3 shows such results for four different energies: 55, 237, 897, and 3,400 keV, which are representative of four distinct populations. This figure reveals distinct energy dependencies of the response of electrons to geomagnetic storms. Below ~100 keV, electrons are enhanced very rapidly at all L-shells (2.5 to 6) during the main phase of storms and then decay quickly during the recovery phase. Electrons with energy in the 100 to a few hundred keV range exhibit behavior like the 237-keV statistics shown in Figure 3. Electrons at a few

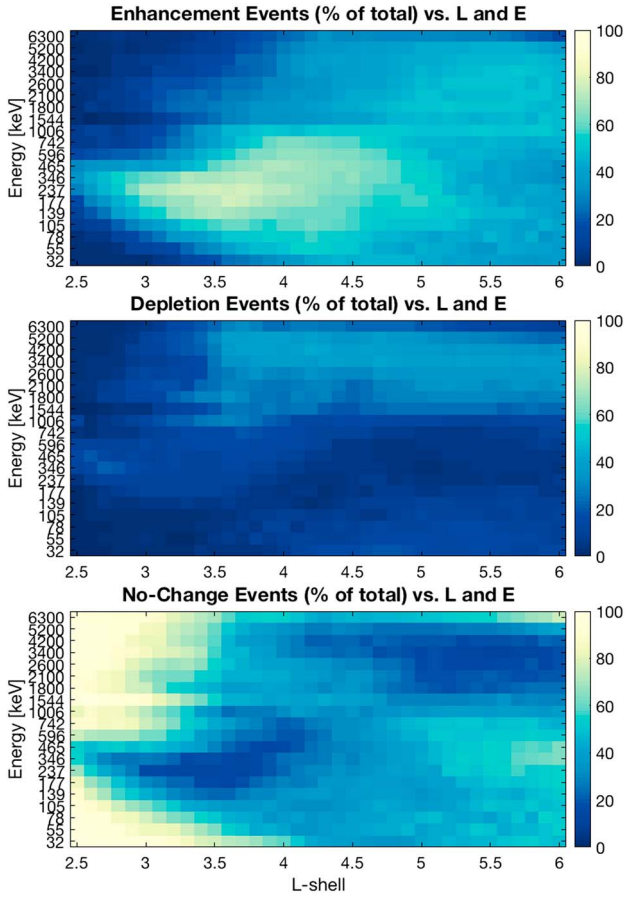

Figure 2. Statistical results of enhancement, depletion, and no-change occurrences. Each panel shows the percentage of all events in color that result in an (top) enhancement, (middle) depletion, or (bottom) no change of radiation belt electrons as a function of L-shell and electron energy. The total of percentages from the three plots for any L-shell and energy bin will yield 100%.

hundred keV are also enhanced in the majority of storms. During the main phase these electrons tend to flood the slot region in the majority of events (e.g., Turner et al., 2016), but any prolonged enhancement is more localized in L-shell as the slot region reforms at L < ~4 during the recovery phase. Relativistic electrons, with energy >~500 keV, are exemplified in the plots for 897 keV and 3.4 MeV in Figure 3. During the main phase of storms, these electrons always experience flux depletions, or "dropouts," throughout the prestorm outer belt. The dropout signatures during the main phase are strongest at higher L-shells, consistent with the storm time dropout described by Turner et al. (2014) and the dropouts during SIR-driven events described in Morley et al. (2010). Depletion events from Figure 2 tend to be those in which the annihilative effect of this main phase dropout at any particular L-shell and energy is never overcome by subsequent flux enhancements. Enhancements occur during the recovery phase of the storms and become less likely for higher-energy electrons. The slot region remains largely devoid of these electrons in the vast majority of events. Any enhancements that do occur for these electrons, as well as recovery to prestorm intensity levels, occur longer into the recovery phase for higher-energy electrons. Interestingly, the peak in poststorm intensity moves to lower L-shells for <1-MeV electrons but to higher L-shells for >1-MeV electrons.

Figure 4 shows yet another way to examine the response of the radiation belt electrons to storms. The background color plots show the mean, median, and upper and lower quartiles of $\log_{10}$(flux) as a function of L-shell and energy at +12-hr epoch time; the gray contour lines correspond to the color plots. The white, dashed contour lines show the prestorm distribution from −48-hr epoch time. These plots show how the outer belt population is enhanced and the slot region is filled during the main phase of storms for tens to hundreds of keV electrons. The relativistic electron outer belt is also enhanced at higher L-shells for most storms but these electrons do not fill the slot region during storm main phase. The effects of flux dropouts throughout the outer belt are also evident for >~1-MeV electrons at +12-hr epoch time (i.e., the gray contours are below the equivalent white contours at these energies), particularly in the mean and lower quartile plots. Comparing and contrasting the quartiles with the mean and median results, it is clear that in the upper quartile, enhancements of electrons at higher energies occur deeper into the slot region (lower L-shells), while the opposite is true for the lower quartile.

The storm time morphology of the electron radiation belts is further detailed in Figure 5. Here mean ($\log_{10}$(-flux)) is shown at −48-hr epoch time, corresponding to the brown contour lines, and different color contours correspond to the state of the belts at different epoch times as labeled in the legend. Figure 5 reveals four key features of the storm time morphology of radiation belt electrons. First, tens to hundreds of keV electrons flood the outer belt and slot region during the main phase (approximately −12 hr < epoch time < +12hr) of most storms and the slot reforms over several days as those electrons decay away again during the recovery phase (approximately epoch time > +12 hr). The slot reformation is dependent on L-shell and energy: at lower energies, the slot is wider and extends to higher L-shells (e.g., L > 4 for 237-keV electrons) and decay times are faster; at higher energies, the slot is narrower and confined to lower L-shells (e.g., L < 3 for 3.4-MeV electrons) and decay times are shorter. Second, <200-keV electrons experience enhancements during the main phase of storms, between −12- and +6-hr epoch time. Third, hundreds of keV electrons experience continued enhancements during the main phase of storms at L > ~4 while they are decaying and the slot reforms at L < 4. Finally, MeV electrons first experience a dropout over the full outer belt during the main phase (−12- to 0-hr epoch time); this dropout is strongest at higher L-shells. MeV electrons recover to higher than prestorm levels (on average) during the recovery phase at all L-shells >~3.5.

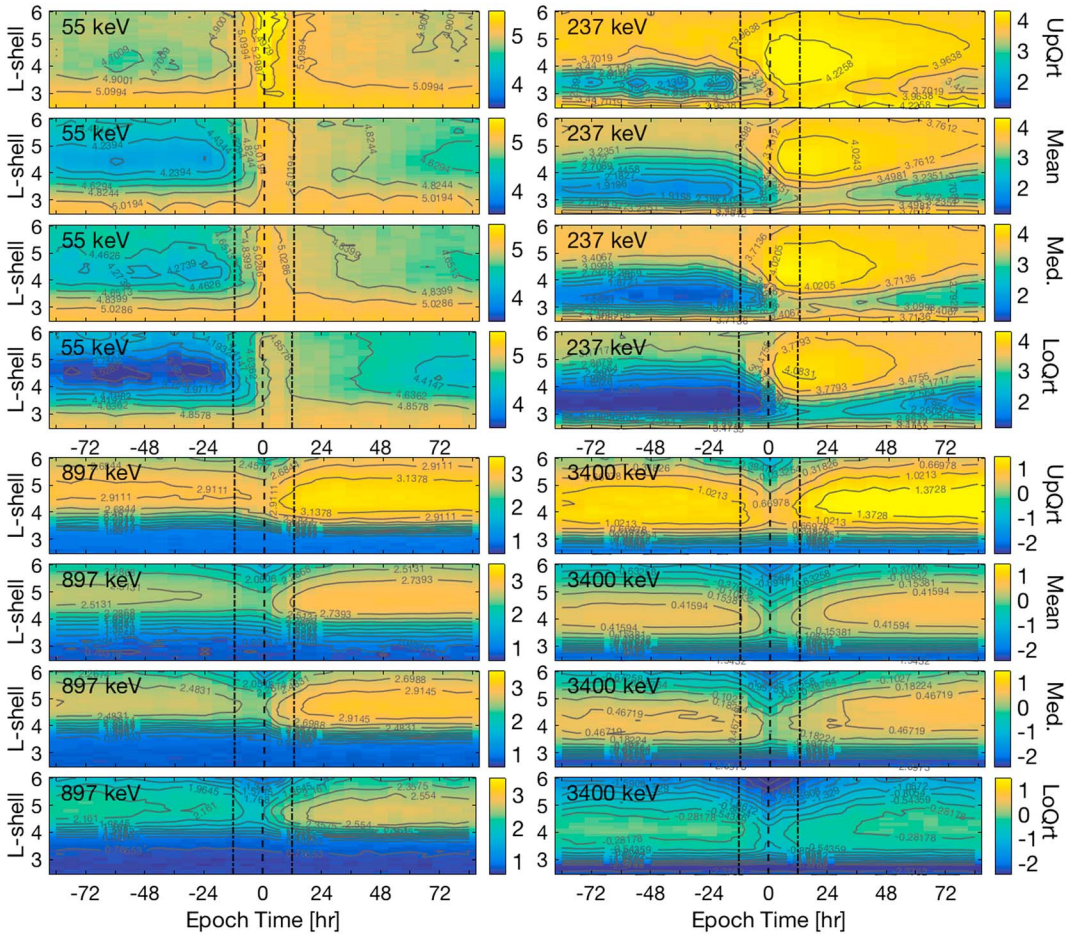

Figure 3. Statistical results of electron fluxes as a function of storm epoch time, L-shell, and energy. Each plot shows statistical quantities of electron fluxes ($\log_{10}$ of flux in color) binned by epoch time and L-shell. Four plots are shown for four different electron energies: 55, 237, 897 keV, and 3.4 MeV, as labeled in the top left of each plot. For each energy, the four plots show from top to bottom the upper quartiles, means, medians, and lower quartiles of fluxes in each epoch time and L-shell bin from all storms. Constant contours of the color scale are superposed in gray for ease in reading. Dashed black lines mark epoch times of −12, 0, and +12 hr, the period during which fluxes were excluded from the enhancement/depletion/no-change analysis. For results shown in this same format for different electron energies, please see the supporting information.

3.3. Storm Time Morphology of Radiation Belt Electrons: Events by Storm-Driver

To investigate how storms driven by different solar wind conditions affect the radiation belts differently, we organized the set of 110 storms by storm-driver in the solar wind. Five driver categories were used: (i) CME sheath only, (ii) CME ejecta only, (iii) full CMEs consisting of both sheath and ejecta, (iv) SIRs, and (v) unclear and complex events including those with multiple driver events in the solar wind. These storm-drivers were identified following the criteria and method described in Kilpua et al. (2015). This categorization resulted in subdivision of the 110 storms as follows: CME sheaths: 11 storms, CME ejecta: 14 storms, full CMEs: 23 storms, SIRs: 47 storms, and unclear/complex: 15 storms. For OMNI data statistics from each type of driver, like that shown in Figure 1, please see plots in the supporting information. Figure 6 shows the statistical response of radiation belt electrons for each of the five storm-driver categories in the same format as Figure 2. These results reveal some interesting similarities and differences.

Comparing Figure 6 to the results highlighted in Figure 2, storms driven by all of these different solar wind structures tend to result in enhancements of hundreds of keV electrons at $3 \leq L \leq 5$, and there is a distinct jump in likelihood of depletions for electrons with energy >~1.5 MeV throughout the outer radiation belt.

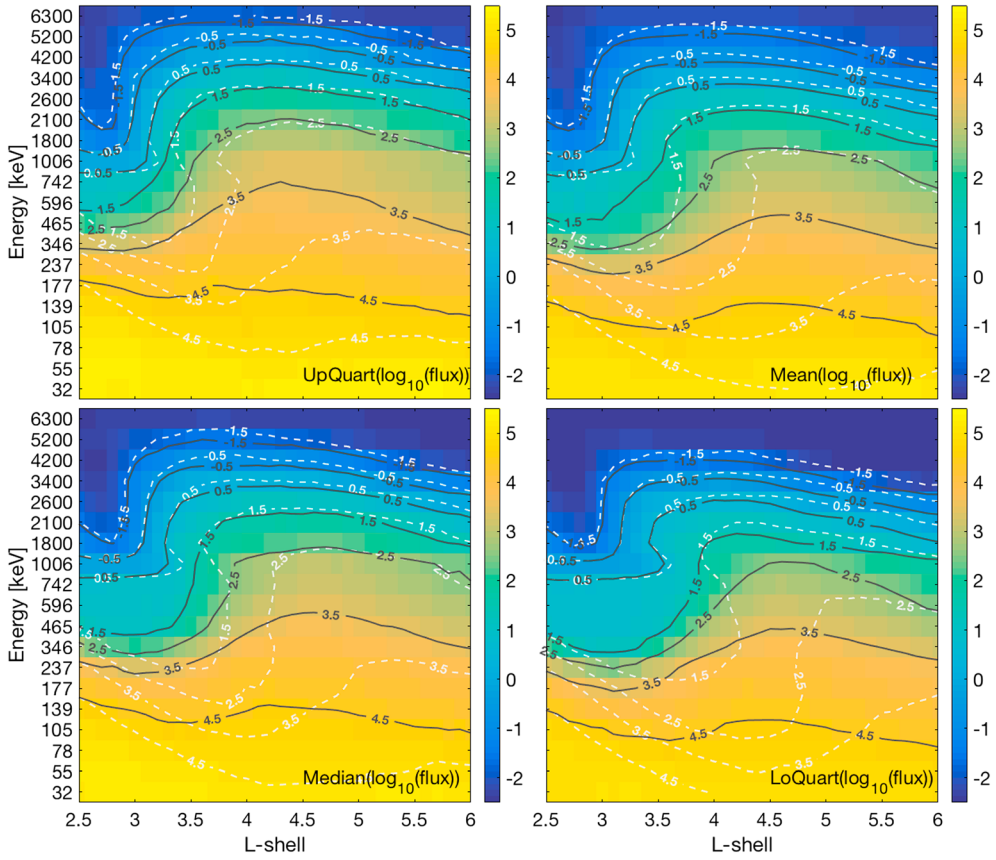

Figure 4. Statistical results of morphology of the electron radiation belts as a function of L-shell, energy, and storm epoch time. Each plot shows statistical quantities of electron fluxes ($\log_{10}$ of flux in color) binned by L-shell and energy. The background color plot shows the results at −48-hr epoch time, with the dashed white contour lines corresponding to that. The solid gray contours show the structure of the belt at +12-hr epoch time. The four plots show (top left) upper quartiles, (top right) means, (bottom left) median, and (bottom right) lower quartiles, as labeled, in each L-shell and energy bin from all storms.

For the same reasons described above, no-change events are most likely for MeV electrons at L < ~3.5, ≥5-MeV electrons at L > ~5, tens to a few hundred keV electrons at L < ~3.5, and hundreds of keV electrons at L > ~5.

There are also some marked differences in the statistical response of the radiation belt electrons when storms are subdivided by storm-driver, as detailed in Figure 6. Full CMEs (sheath + ejecta) are more efficient than other drivers at enhancing MeV electrons at low L-shells (L < ~5), while SIRs are relatively more efficient at enhancing MeV electrons at higher L-shells (L > ~4.5). CME ejecta are particularly efficient for enhancements of <200-keV electrons at L > ~5.5 compared to other drivers. Using approximately 50% as a distinguishing level, storms driven by only CME sheaths or ejecta are most efficient for MeV electron depletions throughout the full range of the outer radiation belt. CME ejecta and SIR-driven events are likely to result in MeV electron losses at L < ~5, while CME sheaths tend to result in losses of MeV electrons throughout the outer belt. Unclear/complex events are particularly effective for depletions of MeV electrons at L > ~4.5. Intriguingly, CME sheath-driven events are especially effective for enhancements of ~500-keV to ~1.5-MeV electrons at L > 5, which we have confirmed is true for many of the events in this category and is not just an anomalous feature from one or two outliers.

Figures 7–9 show the average response to storms driven by different solar wind drivers in the same format as Figure 3. These plots reiterate the points made comparing and contrasting the results from all events (Figure 3) to those categorized by storm-driver. As already shown for Figure 6, storms driven by CME sheaths (Figure 7a) and CME ejecta (Figure 7b) typically result in depletions of ~MeV electrons

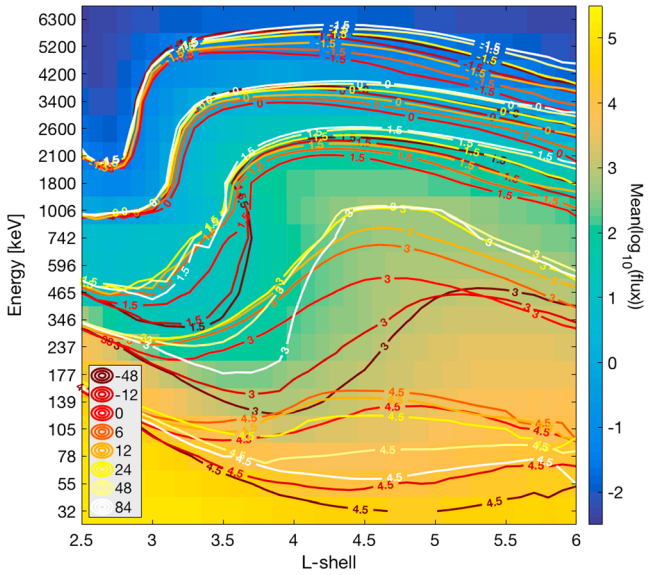

Figure 5. Statistical time history of the morphology of the electron radiation belts during geomagnetic storms. Similar to Figure 4, the color plot shows the mean electron fluxes ($\log_{10}$ of flux in color) from all storms binned by L-shell and electron energy at −48-hr epoch time. The dark brown contour, labeled −48 in the key, corresponds to the color plot. The structure of the belts versus L-shell and energy in this same format are shown at different epoch times with the different color contours, with the corresponding epoch time in hours labeled on the key. This plot effectively shows the average time history of the morphology of the radiation belt electrons during storms.

throughout the outer belt. Losses of MeV electrons in these types of storms begin during the main phase of the storm and are strongest at higher L-shells. Tens to hundreds of keV electrons are typically enhanced by at least an order of magnitude during the main (tens to ~200 keV) and early recovery phases (several hundreds of keV) of these types of storms. By ~36 hr into the recovery phase, CME sheath events are effective at forming (on average) two peaks in intensity of multi-MeV electrons, although the overall intensity of those peaks are still reduced compared to the prestorm population. The innermost of the two belts, around L~3.5, is apparently a remnant leftover from the dropout during the main phase, while the second, outer peak in intensity around L~5 forms one to two days after the start of the early recovery phase.

Figures 8a and 8b show the results for full CME- and SIR-driven storms, respectively. From these plots, it is clear that storms driven by both of these types of solar wind structures result in peak flux enhancements of the radiation belt electrons across the full range of energies, on average. However, there are some notable differences. In both types of storm, the location of the flux peak of several MeV electrons moves to higher L-shells during the recovery phase when compared to before the storms. For SIR-driven storms for 5.2-MeV electrons, like CME sheath-driven events, there is evidence of a remnant belt after the main phase dropout and the formation of a new and distinctly different outer belt (i.e., there are two peaks in the radial distribution of flux), during the early recovery phase. Unlike MeV electrons, relativistic electrons with energy <1 MeV tend to form a new peak location at lower L-shells during the early recovery phase compared to the prestorm distributions.

Results for unclear/complex events are shown in Figure 9. On average, these tend to result in little change to the multi-MeV electron intensities, although their peak flux locations move to lower L-shells. As was also typical of the other four types of drivers, <1-MeV electrons are enhanced on average during the main and early recovery phase of the unclear/complex driver events. Two distinct features are common to all five types of driver event: dropouts of relativistic (>~500 keV) electrons occur throughout the outer belt during the main phase of storms in all five driver categories; enhancements of tens to ~200-keV electrons occur and extend into the inner radiation belt during the main phase of storms driven by all types of solar wind drivers.

The morphology of the electron radiation belts during geomagnetic storms driven by different solar wind drivers can be further examined with Figure 10. Like that shown for all storms in Figure 5, the plots in Figure 10 show the mean prestorm state of the electron radiation belts versus L-shell and energy plus the time history (in colored contours) of how the belts evolve through the different sets of storms. Some key features of these results include that in the average prestorm period, the inner radiation belt extends to higher L-shells for lower energy electrons while the slot region is broader and extends to higher L-shells for lower energy electrons. In storms driven by all five categories of event, tens to hundreds of keV, though notably not ≥1 MeV, electrons flood the slot region during the main and early recovery phases of the storms. The slot subsequently reforms for these electrons during the remainder of the recovery phase, resulting in a poststorm structure that is morphologically very similar to the prestorm structure albeit at significantly enhanced levels. Provided quiet conditions over more time after the storms (not shown), the structure of the electron radiation belts returns to the average prestorm state. Also in all five categories, MeV electrons throughout the outer belt dropout during the main phase of the storms.

Differences from each type of driver include that CME sheath and ejecta only events result in poststorm depletions of MeV electrons near the peak intensity locations at L < 5, on average, but for CME sheath and CME ejecta events, multi-MeV electrons end up slightly enhanced and returning to prestorm average levels, respectively, at higher L-shells (L > ~4.5) by the end of the storms (e.g., 84-hr epoch time shown with the white contours). As previously described, full CME events typically result in an enhancement of electrons at all energies in the outer belt, with the enhancements for multi-MeV electrons being most

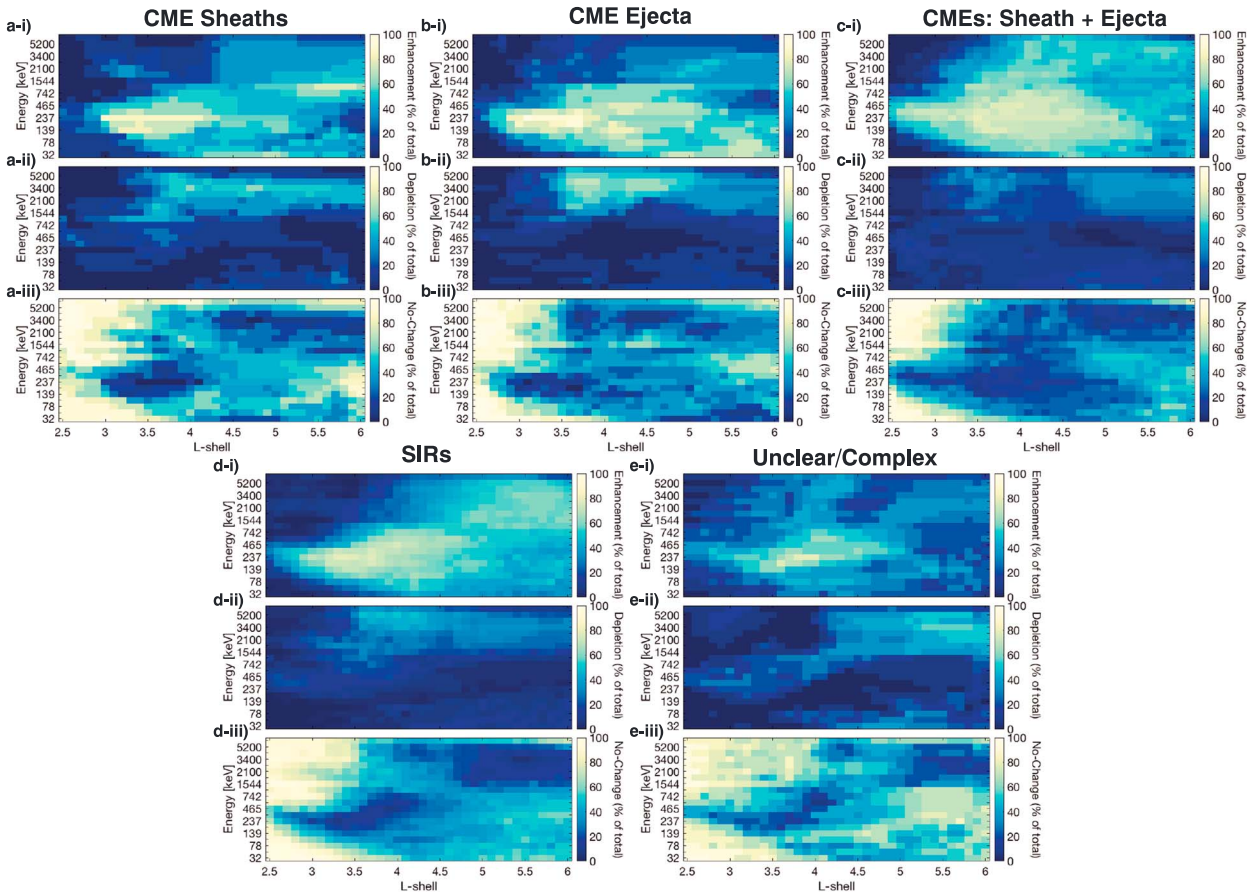

Figure 6. Statistics of the radiation belt electron response to geomagnetic storms driven by different events in the solar wind. Five versions of the plots from Figure 2 are shown here, one for storms driven by each of the following types of solar wind structure: (a) CME sheaths, (b) CME ejecta, (c) full CMEs (consisting of both shocks/sheaths and ejecta), (d) SIRs, and (e) unclear or complex events. For these five categories, results are shown in the same format as Figure 2. See corresponding text for additional details.

pronounced at lower L-shells (i.e., L < ~5). SIR-driven events also typically result in an enhancement of outer belt electrons, but the enhancements of multi-MeV electrons are most pronounced at higher L-shells, L > ~4.5. SIR-driven events tend to result in the formation of remnant belts at L < 4 and a second peak in the intensity of multi-MeV electrons (>~4 MeV) at L > 4 during the recovery phase (e.g., see peaks in the −1.5 contours for +24-, +48-, and +84-hr epoch time (yellow and white contours) at L~3.8 and L~4.7 in Figure 10d). CME sheath events also tend to result in remnant belts and two distinct intensity peaks in the outer belt for multi-MeV electrons (e.g., see peaks in the −1.5 contours for +48- and +84-hr epoch time (light yellow and white contours) at L~3.8 and L~4.6 in Figure 10a). Unclear and complex drivers tend to result in radiation belt morphology similar to that for full CMEs.

4. Discussion

This study represents a progression from the work of O'Brien et al. (2003), Reeves et al. (2003), Kilpua et al. (2015), Turner, O'Brien, et al. (2015), Moya et al. (2017), Murphy et al. (2018), and several others. Unlike those studies, this study combines results from both the Van Allen Probes' MagEIS and REPT instruments, includes a larger number of events, and examines statistics of the morphology of radiation belt electrons during storms. By examining the full statistical ranges (e.g., means, medians, quartiles) of electron intensity throughout the belt as a function of energy, L-shell, and storm epoch time, these results offer a model for quantifying the range of possible responses of radiation belt electrons to geomagnetic storms. While the complexity of a “delicate and complicated balance” (Reeves et al., 2003, pp. 36–1) of source and loss remains valid, examining results like this from Van Allen Probes removes much of the mystery of the response of

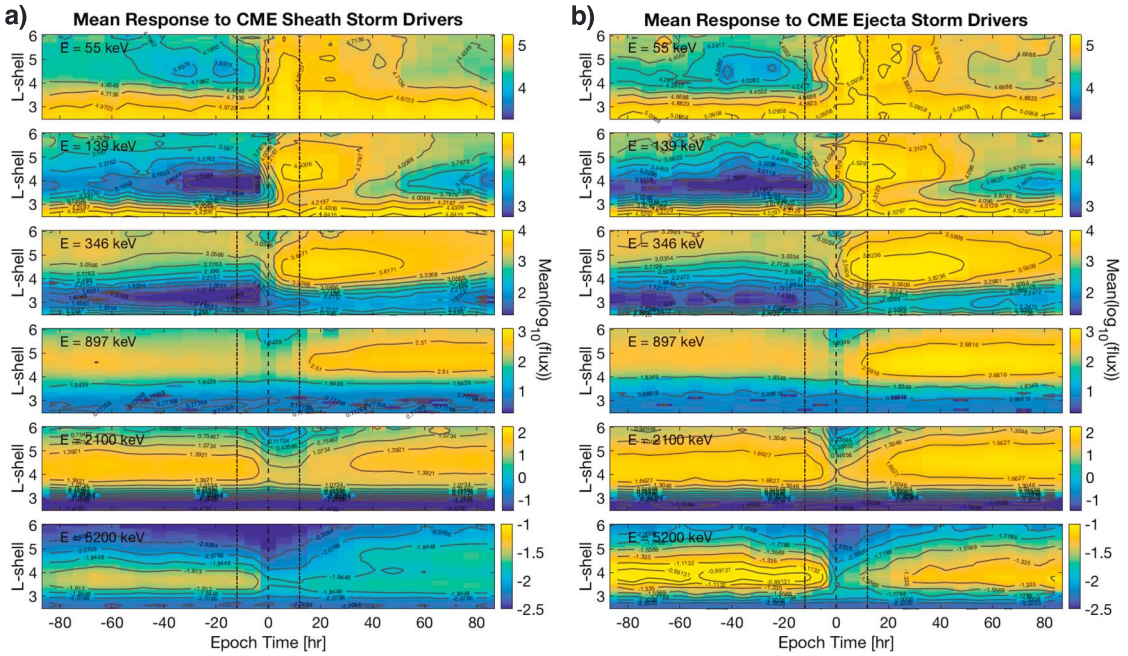

Figure 7. Mean response of radiation belt electrons to geomagnetic storms driven by (a) CME sheaths and (b) CME ejecta. Each plot shows the mean of electron fluxes ($\log_{10}$ of flux in color) from all storms in each driver category as a function of epoch time (x axis), L-shell (y axis), and energy (column of six plots). Results for 55-, 139-, 346-, 897-keV, and 2.1- and 5.2-MeV electrons are shown, as labeled in the top left of each color plot. For results shown in this same format for different statistical quantities, please see the supporting information.

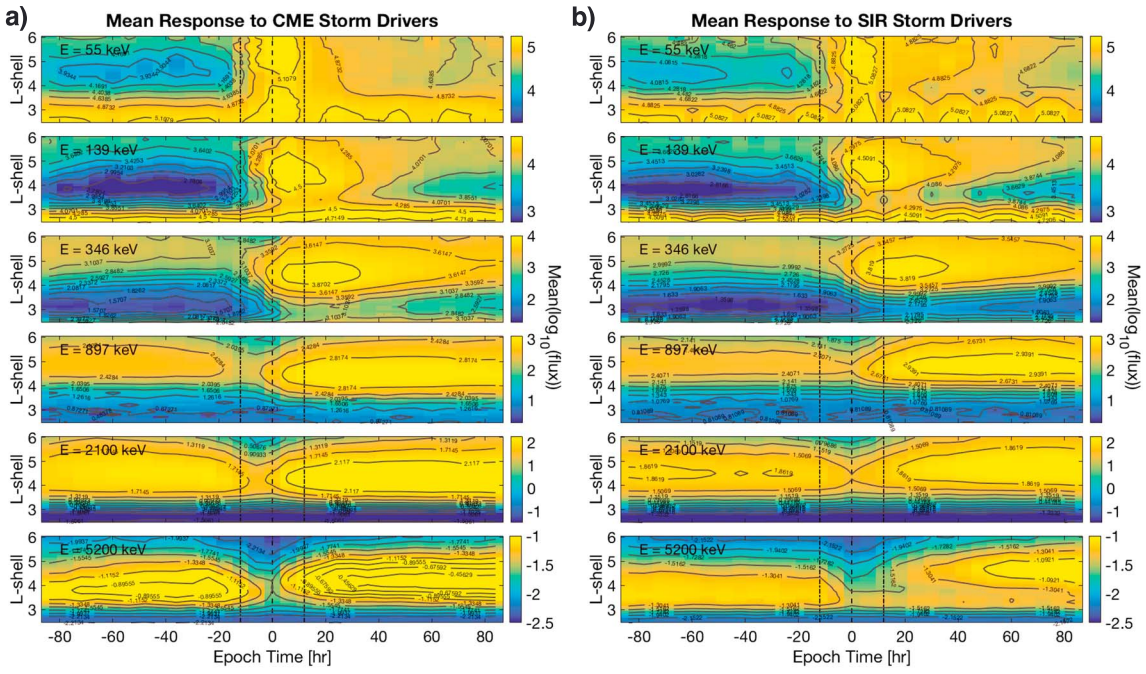

Figure 8. The same as in Figure 7 but for the subset of storms driven by (a) full CMEs and (b) SIRs. For results shown in this same format for different statistical quantities, please see the supporting information.

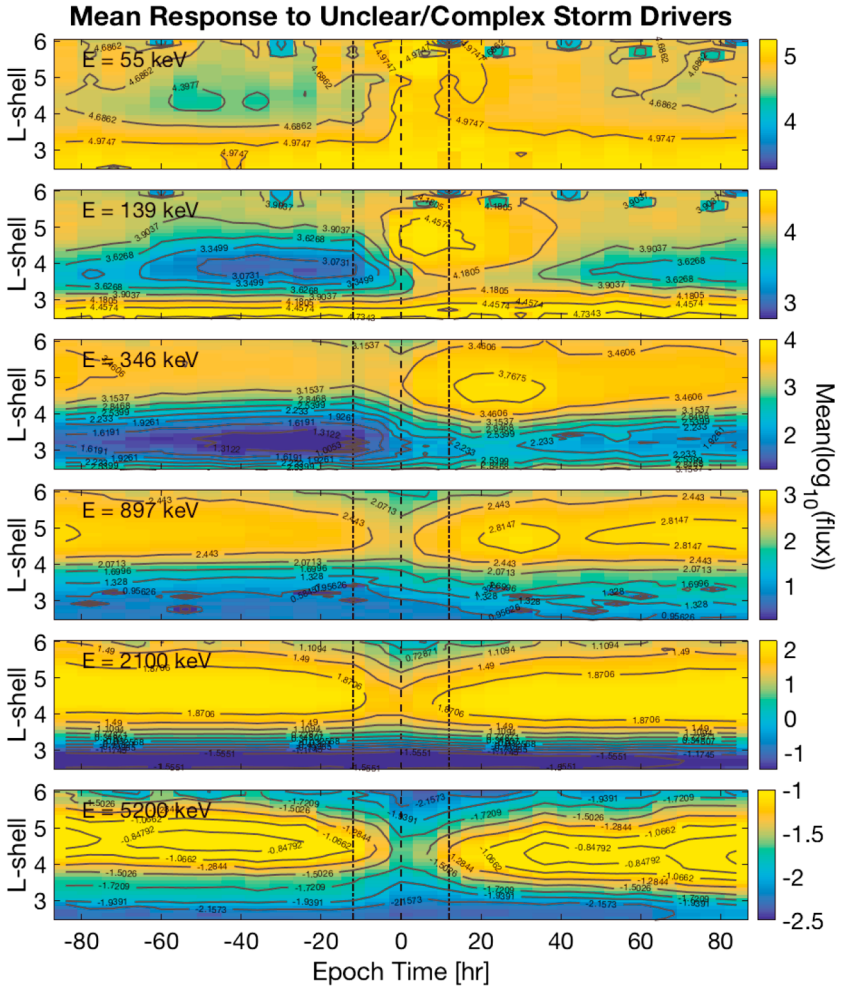

Figure 9. The same as in Figure 7 but for the subset of storms driven unclear or complex solar wind structures. For results shown in this same format for different statistical quantities, please see the supporting information.

radiation belt electrons from storm to storm. In particular, while there are many similarities, there are also some distinctive differences between the electron radiation belts' response during geomagnetic storms driven by different types of events in the solar wind.

When the 110 storms examined here were organized by five distinct storm-drivers (CME sheaths only, CME ejecta only, full CMEs with both sheath and ejecta regions, SIRs, and unclear/complex events), it emerged that full CMEs are particularly effective at driving enhancements of multi-MeV electrons at lower L-shells (L < ~5), while SIRs are particularly effective at driving enhancements of multi-MeV electrons at higher L-shells (L > ~4.5), which is consistent with recent results from LEO reported in Benacquista et al. (2018). This result for SIRs is also consistent with results from spacecraft at GEO, showing that SIR-driven storms are efficient for enhancements of MeV electrons at GEO (e.g., Borovsky & Denton, 2006; Kilpua et al., 2015; Miyoshi et al., 2013). SIR-driven storms have prolonged recovery phases, often with enhanced *AE* levels, as the HSS in the solar wind continues to interact with the magnetosphere; thus, activity that is statistically preferable for radiation belt enhancements tends to be prolonged for SIR events. Full CMEs and complex-driver events are more effective at enhancements of electrons within the slot region when compared to SIR events (e.g., Figure 10); this implies that CMEs and complex events are most effective for radiation belt electron source (loss) processes at lower (higher) L-shells, which is consistent with Shen et al. (2017) plus the results of Tverskaya et al. (2003) and Zhao and Li (2013) since CMEs typically result in stronger geomagnetic storms (quantified by *Dst* or *SYM-H*) than SIR-driven events. We speculate that this effect may

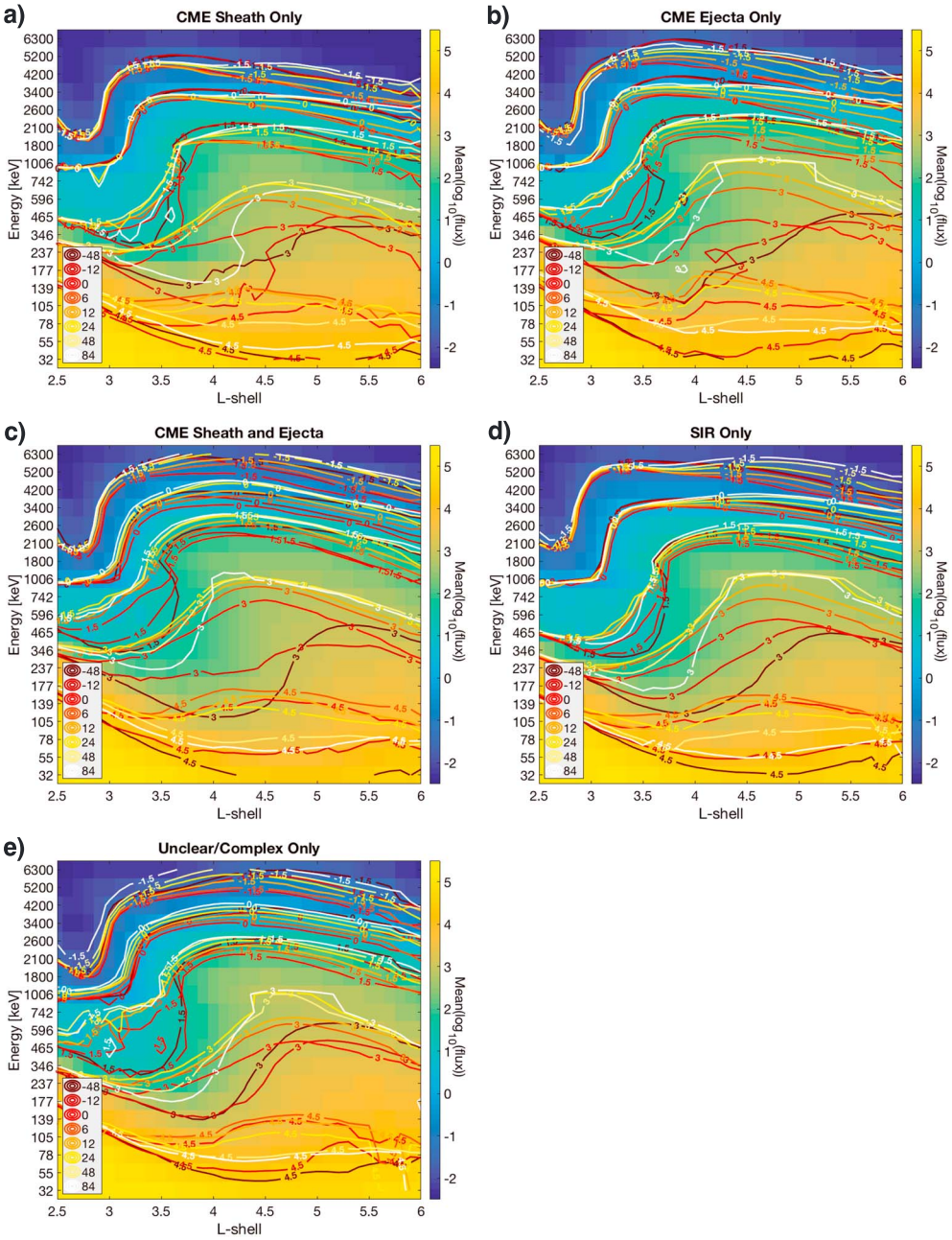

Figure 10. Statistical time history of the morphology of the electron radiation belts during geomagnetic storms driven by different solar wind structures. Each of the five plots shows the same as in Figure 5 but for the subset of storms driven by (a) CME sheaths, (b) CME ejecta, (c) full CMEs, (d) SIRs, and (e) unclear/complex solar wind structures.

result from CMEs more effectively compressing the magnetosphere, often involving shock injections to lower L-shells, and more effectively eroding the plasmasphere enabling wave-particle interactions (e.g., with chorus and/or ULF waves) to occur at lower L-shells. Events driven by CME sheaths or CME ejecta are particularly effective at causing depletions of ≥1.5-MeV electrons throughout the outer belt. That result is consistent with the results of Hietala et al. (2014) and Kilpua et al. (2015); those studies concluded that loss in such storms possibly results from solar wind conditions characteristic of those driver events being particularly effective at driving losses of outer belt electrons to the magnetopause and outward radial transport while simultaneously being ineffective at driving acceleration of outer belt

electrons. Intriguingly, storms driven by CME sheaths also result in a distinct likelihood of enhancements of ~1-MeV electrons at L > 5.

Another distinct difference between radiation belt responses to storms with different solar wind drivers is that CME sheath and SIR storms preferentially resulted in two distinct peaks of intensity of multi-MeV electrons in the outer radiation belt. Such structures were reported by Baker, Kanekal, Hoxie, Henderson, et al. (2013) and Turner et al. (2013). According to Turner, et al. (2013), Shprits et al. (2013), Thorne, Li, Ni, Ma, Bortnik, Baker, et al. (2013), Thorne, Li, Ni, Ma, Bortnik, Chen, et al. (2013), and Mann et al. (2016), the following scenario has been proposed to explain these double outer belt structures. After outer belt dropout events during magnetospherically active periods, often a remnant belt is leftover at low L-shells (L < ~4) after the loss processes responsible for the dropout subside. During this period of loss activity when the remnant belt is formed, the plasmasphere typically erodes and then refills, with the plasmapause moving to higher L-shells than that of the peak in remnant belt intensity. If the solar wind driver of all this activity is also effective at driving acceleration of outer belt electrons after the dropout, a new outer belt can form at higher L-shells than the plasmapause. That new belt forms the outermost peak in intensity while the remnant belt is the innermost intensity peak in these double outer belt structures. Due to the energy- and L-shell-dependent role of losses by interaction with hiss waves within the plasmasphere (e.g., Thorne, Li, Ni, Ma, Bortnik, Baker, et al., 2013; Thorne, Li, Ni, Ma, Bortnik, Chen, et al., 2013; Ripoll et al., 2016; see discussion below), the remnant belt will quickly erode for hundreds of keV electrons but will persist for days or weeks for multi-MeV electrons. The fact that these remnant belts of MeV electrons appear in the statistical results for SIR-driven storms is consistent with that scenario due to the typical magnetospheric response to SIRs. SIR-driven storms are typically not as strong as their CME counterparts (e.g., Borovsky & Denton, 2006). From Kilpua et al. (2015), CME ejecta and full CMEs tend to include prolonged periods of southward IMF B_z, while SIRs and CME sheath events do not. Thus, in SIR-driven storms, the plasmapause may not be eroded to very low L-shells and subsequent acceleration beyond the plasmapause can occur at higher L-shells.

There are also multiple responses of radiation belt electrons that are generally common to all storms. MeV electrons typically display dropouts throughout the outer belt during storm main phase and then a period of replenishment during the early recovery phase. Whether the source activity responsible for that replenishment is enough to result in an enhancement of MeV electrons at any particular L-shell varies from storm to storm but has some dependency on storm-driver, as described above. This MeV electron response is consistent with the results of Murphy et al. (2018), who found that there was a repeatable sequence of behavior for outer radiation belt electrons during storms. Recall that Murphy et al. (2018) described two distinct behaviors of relativistic outer belt electrons organized by storm phase: predominant loss during storm main phase and predominant rapid acceleration during storm recovery phase. Our results are consistent: whether relativistic electrons in the outer belt are enhanced or not as a result of storm activity depends on the relative intensity of loss during the main phase and acceleration during the recovery phase.

Another general electron response common to storms is that <600-keV electrons are enhanced in the inner part of the outer belt and the slot region (L < 5) in the vast majority (~90%) of geomagnetic storms. This behavior was also reported by Turner, O'Brien, et al. (2015). It is still unknown what drives such rapid enhancements down to such low L-shells (L < 2.5); they occur too quickly for radial diffusion, cannot simply result from enhanced global convection since they occur within the plasmasphere (e.g., Turner, Claudepierre, et al., 2015), and are not observed for protons at the same energy (e.g., Zhao et al., 2016). However, such electron enhancements are important: Turner et al. (2016) argued that these enhancements may be the dominant source of hundreds of keV electrons in the inner radiation belt. Lejosne et al. (2018) argued that the electric fields associated with subauroral polarization streams may be responsible for such electron enhancements at low L-shells. Regardless of what drives them, the results presented here reveal that their occurrence is typical during the main phase of geomagnetic storms.

The results displayed here in Figures 4, 5, and 10 build upon those of Reeves et al. (2016) and Ripoll et al. (2016, 2017). From a period in March 2013, Reeves et al. (2016) introduced the energy and L-shell dependencies on the structure of the inner and outer radiation belts and slot region and how this structure of the electron radiation belts evolved over the course of one storm. This evolution involved the flooding of the slot region by tens to hundreds of keV electrons, a subsequent enhancement of relativistic electrons in the outer belt, and then slow, energy- and L-shell-dependent decay and reformation of the slot for the tens to hundreds

of keV electrons. The reformation of the slot during that period in March 2013 was shown by Ripoll et al. (2016, 2017) to be entirely consistent with losses by plasmaspheric hiss waves during the recovery phase and geomagnetically quiet period after the storm. The statistics from the 110 storms presented here reveal that global radiation belt morphology described by Reeves et al. (2016) and Ripoll et al. (2016, 2017) is typical behavior of the electron radiation belts during storm time magnetospheric activity.

Another interesting feature from this statistical analysis is the distinct jump in the likelihood of depletions throughout the outer belt for $E \geq 1.5$-MeV electrons (see Figures 2 and 6). One mechanism that could possibly be responsible for this feature is wave-particle interactions between multi-MeV electrons and electromagnetic ion cyclotron (EMIC) waves. EMIC waves have been identified as an important loss mechanism for outer radiation belt electrons (e.g., Thorne 2010), but the interaction process is highly dependent on electron energy and pitch angle plus plasma ion composition. In Earth's inner magnetosphere, only very energetic electrons with energy typically in the MeV range are able to overtake and anomalously resonate with EMIC waves (e.g., Meredith et al., 2003; Ukhorskiy et al., 2010), but such interactions can cause rapid pitch angle scattering of electrons into the atmospheric loss cone. Aseev et al. (2017) and Shprits et al. (2017) both showed evidence in support of this loss mechanism for multi-MeV electrons. In any particular event, losses by EMIC waves are likely localized in L-shell due to the nature of EMIC wave activity and electron precipitation structures (e.g., Blum et al., 2013; Blum et al., 2017), but statistically over many events the localized nature should smear out in L-shell, and we speculate that losses by EMIC waves might result in the higher likelihood of multi-MeV electron depletions throughout the outer belt as shown in Figures 2 and 6.

There are several possible improvements that can be made for continuing and future studies like this one. This study should be repeated after the end of the Van Allen Probes mission to ensure that the statistics are as comprehensive as possible. With more storms, it will be interesting to further subcategorize solar wind driving conditions based on the polarity and magnitude of IMF B_z and fast versus slow solar wind during the recovery phase (e.g., Kilpua et al., 2015). The analysis can be further refined by using more complicated, multiple epoch time designations specific to the storm phase (e.g., Katus et al., 2013) and/or the nature of each type of driver (e.g., Kilpua et al., 2015). Data could also be organized in L-shell in relation to the location of the plasmapause, similar to what was done with hiss by Malaspina et al. (2016). To further investigate the possible role of EMIC waves in driving depletions of multi-MeV electrons throughout the outer belt, pitch angle resolved electron data could be employed instead of just the omnidirectional fluxes used here. This study could be repeated using electron phase space density as a function of the adiabatic invariants instead of omnidirectional flux as a function of energy and L-shell. Another interesting modification would involve comparing the poststorm fluxes (or phase space density) to long-term averages compiled from nonstorm conditions. That modification would account for the fact that losses of relativistic electrons during the main phase of storms effectively "reset" the outer belt, such that the poststorm populations are mostly unrelated to the prestorm ones (e.g., Turner et al., 2014). With these results and more from future events, a neural network model (e.g., Bortnik et al., 2018) could be developed to predict the storm time response of radiation belt electrons throughout the radiation belts. Finally, the analysis conducted here (and those suggestions just listed) can be repeated using Van Allen Probes data for other radiation belt events such as nonstorm enhancements and depletions and dropouts.

5. Summary and Conclusions

There were 110 isolated geomagnetic storms with *SYM-H* minima <-50 nT during the five-year period from Van Allen Probes launch in September 2012 through September 2017. In this study, we examined the statistical response of Earth's radiation belt electrons to those 110 events using Van Allen Probes MagEIS and REPT data. Unlike the results for MeV electrons at GEO alone, the results organized by energy, L-shell, and storm epoch time revealed some qualitatively predictable behavior. In particular, the storm time morphology of the radiation belt electrons described in Reeves et al. (2016) is generally true during most geomagnetic storms: (i) the prestorm belt exhibits the classic two-belt structure for tens of keV to ~1-MeV electrons, with the outer edge of the inner belt extending to higher L-shells and the slot region being wider for electrons at lower energies in that range; (ii) during the main phase of the storm, the slot region is flooded with a new population of tens to a few hundred keV electrons while many hundreds of keV to several MeV electrons exhibit a dropout throughout most if not all of the outer radiation belt; and (iii) during the recovery

phase, energy-dependent loss removes the tens to hundreds of keV electrons at lower L-shells, reforming the slot over a few days, while >1-MeV electrons become enhanced somewhere within the outer radiation belt in the majority of events. As described by Lyons and Thorne (1973) and Ripoll et al. (2016, 2017), plasmaspheric hiss plays a critical role in the reformation of the slot for tens to hundreds of keV electrons as the plasmasphere rebuilds after a storm. Multi-MeV electrons are the least predictable, with nearly equal chance of being enhanced as depleted or relatively unchanged from prestorm to poststorm levels. Consistent with the results described by Murphy et al. (2018), however, in the vast majority of storms, multi-MeV electrons first exhibit a dropout during the main phase followed by some replenishment due to some source active during the recovery phase. There is also a marked increase in the likelihood of depletions for several MeV electrons during storms, which we speculate may be due to the energy-dependent role of EMIC wave scattering electrons into Earth's atmospheric loss cones.

The statistical responses become more distinct when the type of solar wind storm driver is considered. Full CME storms are especially effective at causing enhancements of multi-MeV electrons at lower L-shells, $L < \sim 5$, while SIR-driven storms are especially effective at causing enhancements of multi-MeV electrons at higher L-shells ($L > \sim 4.5$). Storms driven by partial CMEs, either CME sheaths or CME ejecta only, are most likely to drive prolonged depletions of multi-MeV electrons throughout the outer belt. Interestingly, however, CME sheaths also result in a higher chance of ~1-MeV enhancements at $L > 5$; that result is quite unexpected and not due to a single outlier event skewing the results. CME sheath and SIR events are also particularly effective at creating outer belt structures with two distinct peaks in intensity (a remnant belt at lower L-shells and a distinct new outer belt at higher L) for multi-MeV electrons, likely due to the effect of their distinct solar wind conditions on the creation of the remnant belt and evolution of the plasmasphere.

The results presented here represent a statistical model for Earth's radiation belt electrons' response to geomagnetic storms as a function of energy, L-shell, and storm epoch time organized by the *SYM-H* index. Future work can include repeating the methodology employed for this study with other types of events (e.g., outer belt enhancements, prolonged periods of substorm activity), further refining the solar wind driver conditions with a larger set of storms, employing multiple epoch times and normalized phases between them (e.g., Katus et al., 2013; Kilpua et al., 2015), and developing a predictive model based on the results. With Van Allen Probes data, the storm time response of Earth's radiation belt electrons is less mysterious and displays some statistically significant repeatable features. However, like Reeves et al. (2003) concluded from results at GEO alone, the response of multi-MeV electrons does indeed appear to be from some highly sensitive competition between source and loss mechanisms active throughout the outer belt during storm main and recovery phases. Additional work is required to better determine why exactly sources dominate over losses in some events while losses dominate over sources in others. To properly address that critical question, it will require having a constellation of radiation belt monitors in near-equatorial GEO-transfer orbits (like Van Allen Probes, to measure the full trapped population and waves) and at low-Earth orbit (to measure precipitation losses) simultaneously spread over a range of local times.

Appendix A: List of Storm Events

Table A1

Number	*SYM-H* Minimum Date	Minimum *SYM-H*
1.	01/10/2012/03:52	−1.38e + 02
2.	09/10/2012/02:10	−1.16e + 02
3.	13/10/2012/07:59	−1.06e + 02
4.	01/11/2012/20:01	−6.80e + 01
5.	14/11/2012/07:27	−1.18e + 02
6.	17/01/2013/18:19	−5.80e + 01
7.	26/01/2013/22:19	−6.20e + 01
8.	01/03/2013/10:12	−7.60e + 01
9.	17/03/2013/20:28	−1.32e + 02

Table A1 *(continued)*

Number	*SYM-H* Minimum Date	Minimum *SYM-H*
10.	21/03/2013/03:54	−6.80e + 01
11.	29/03/2013/16:17	−6.40e + 01
12.	24/04/2013/18:11	−5.20e + 01
13.	01/05/2013/19:10	−6.70e + 01
14.	18/05/2013/03:40	−6.70e + 01
15.	25/05/2013/05:46	−6.50e + 01
16.	01/06/2013/07:48	−1.37e + 02
17.	06/06/2013/23:56	−6.30e + 01
18.	29/06/2013/06:36	−1.11e + 02
19.	06/07/2013/08:33	−8.00e + 01
20.	10/07/2013/07:35	−5.70e + 01
21.	14/07/2013/23:25	−7.70e + 01
22.	05/08/2013/02:20	−5.60e + 01
23.	16/08/2013/04:29	−5.40e + 01
24.	27/08/2013/21:43	−6.40e + 01
25.	02/10/2013/06:19	−9.00e + 01
26.	08/10/2013/22:25	−6.10e + 01
27.	15/10/2013/03:18	−5.20e + 01
28.	30/10/2013/23:20	−5.70e + 01
29.	08/12/2013/08:30	−7.20e + 01
30.	19/02/2014/08:23	−1.27e + 02
31.	23/02/2014/22:48	−6.30e + 01
32.	27/02/2014/23:24	−1.01e + 02
33.	12/04/2014/08:32	−9.22e + 01
34.	30/04/2014/09:10	−7.60e + 01
35.	04/05/2014/05:58	−5.80e + 01
36.	08/05/2014/08:50	−6.20e + 01
37.	08/06/2014/06:50	−7.20e + 01
38.	27/08/2014/18:18	−9.00e + 01
39.	12/09/2014/23:03	−9.70e + 01
40.	09/10/2014/06:20	−5.00e + 01
41.	14/10/2014/18:38	−5.20e + 01
42.	20/10/2014/17:10	−5.70e + 01
43.	28/10/2014/01:52	−5.80e + 01
44.	10/11/2014/17:07	−6.30e + 01
45.	16/11/2014/07:24	−5.10e + 01
46.	22/12/2014/05:25	−6.50e + 01
47.	04/01/2015/16:42	−7.90e + 01
48.	07/01/2015/11:00	−1.35e + 02
49.	26/01/2015/10:30	−5.40e + 01
50.	02/02/2015/06:35	−5.20e + 01
51.	17/02/2015/23:55	−7.00e + 01
52.	24/02/2015/03:36	−7.60e + 01
53.	02/03/2015/08:51	−7.00e + 01
54.	17/03/2015/22:47	−2.34e + 02
55.	11/04/2015/09:36	−8.90e + 01
56.	16/04/2015/23:29	−8.80e + 01
57.	13/05/2015/06:59	−9.80e + 01
58.	19/05/2015/02:55	−6.40e + 01
59.	08/06/2015/07:45	−1.05e + 02
60.	23/06/2015/04:24	−2.08e + 02
61.	05/07/2015/04:52	−5.80e + 01
62.	13/07/2015/10:54	−7.10e + 01
63.	23/07/2015/07:28	−8.30e + 01
64.	31/07/2015/02:59	−5.20e + 01
65.	16/08/2015/07:37	−9.40e + 01
66.	23/08/2015/08:34	−6.20e + 01
67.	27/08/2015/20:32	−1.01e + 02
68.	09/09/2015/08:03	−1.13e + 02
69.	20/09/2015/11:05	−8.40e + 01
70.	04/10/2015/07:33	−5.20e + 01

Table A1 *(continued)*

Number	*SYM-H* Minimum Date	Minimum *SYM-H*
71.	07/10/2015/22:23	−1.24e + 02
72.	14/10/2015/06:05	−5.20e + 01
73.	07/11/2015/06:05	−1.06e + 02
74.	14/12/2015/19:04	−6.00e + 01
75.	20/12/2015/22:49	−1.70e + 02
76.	31/12/2015/23:56	−9.90e + 01
77.	20/01/2016/16:42	−9.50e + 01
78.	03/02/2016/02:52	−6.00e + 01
79.	18/02/2016/00:28	−6.00e + 01
80.	06/03/2016/21:20	−1.10e + 02
81.	16/03/2016/23:41	−6.90e + 01
82.	02/04/2016/22:49	−6.60e + 01
83.	08/04/2016/00:27	−6.70e + 01
84.	13/04/2016/01:09	−7.00e + 01
85.	16/04/2016/20:47	−6.40e + 01
86.	08/05/2016/08:15	−1.05e + 02
87.	06/06/2016/06:47	−5.50e + 01
88.	25/07/2016/17:17	−5.10e + 01
89.	03/08/2016/06:49	−6.30e + 01
90.	23/08/2016/21:13	−8.30e + 01
91.	02/09/2016/01:53	−7.40e + 01
92.	29/09/2016/09:32	−6.40e + 01
93.	13/10/2016/23:45	−1.14e + 02
94.	25/10/2016/22:57	−8.10e + 01
95.	29/10/2016/07:25	−7.80e + 01
96.	03/11/2016/08:51	−5.20e + 01
97.	10/11/2016/15:21	−5.50e + 01
98.	25/11/2016/06:38	−5.30e + 01
99.	21/12/2016/15:41	−5.20e + 01
100.	01/03/2017/22:17	−7.40e + 01
101.	27/03/2017/14:45	−8.60e + 01
102.	04/04/2017/07:06	−5.00e + 01
103.	22/04/2017/23:58	−5.30e + 01
104.	28/05/2017/07:13	−1.42e + 02
105.	16/07/2017/15:51	−6.70e + 01
106.	23/08/2017/12:35	−5.20e + 01
107.	31/08/2017/11:48	−6.40e + 01
108.	08/09/2017/01:10	−1.46e + 02
109.	13/09/2017/00:12	−6.50e + 01
110.	28/09/2017/05:58	−7.40e + 01

Acknowledgments
The authors are thankful to all of the Van Allen Probes, ACE, Wind, OMNI, and Kyoto World Data Center for Geomagnetism teams for making their data available to the public. In addition to coauthors' contributions, we thank from ACE, Wind, and OMNI: J. H. King and N. Papatashvilli and team for the OMNI solar wind data and NASA CDAWeb and mission specific online databases. D.L.T. would like to thank A. Kellerman and A. Drozdov for the useful discussions. Van Allen Probes data are available at <http://rbspgway.jhuapl.edu/data_instrumentation SOC>. We thank the software development teams for SPEDAS <http://themis.ssl.berkeley.edu/software.shtml> and Haje Korth at JHU/APL for the Geopack library. H.H. is thankful for support from The Turku Collegium for Science and Medicine. This work was supported by funding from NASA (Van Allen Probes contract NAS5-01072). EK acknowledges the Finnish Centre of Excellence in Research of Sustainable Space (Academy of Finland grant number 1312390), the European Research Council (ERC) under the European Union's Horizon 2020 Research and Innovation Programme Project SolMAG 4100103, and Academy of Finland Project 1310445.

References

Anderson, B. R., Millan, R. M., Reeves, G. D., & Friedel, R. H. W. (2015). Acceleration and loss of relativistic electrons during small geomagnetic storms. *Geophysical Research Letters*, *42*, 10,113–10,119. https://doi.org/10.1002/2015GL066376

Aseev, N. A., Shprits, Y. Y., Drozdov, A. Y., Kellerman, A. C., Usanova, M. E., Wang, D., & Zhelavskaya, I. S. (2017). Signatures of ultra-relativistic electron loss in the heart of the outer radiation belt measured by Van Allen Probes. *Journal of Geophysical Research: Space Physics*, *122*, 10,102–10,111. https://doi.org/10.1002/2017JA024485

Baker, D. N., Jaynes, A. N., Kanekal, S. G., Foster, J. C., Erickson, P. J., Fennell, J. F., Blake, J. B., et al. (2016). Highly relativistic radiation belt electron acceleration, transport, and loss: Large solar storm events of march and June 2015. *Journal of Geophysical Research: Space Physics*, *121*, 6647–6660. https://doi.org/10.1002/2016JA022502

Baker, D. N., Jaynes, A. N., Turner, D. L., Nakamura, R., Schmid, D., Mauk, B. H., Cohen, I. J., et al. (2016). A telescopic and microscopic examination of acceleration in the June 2015 geomagnetic storm: Magnetospheric multiscale and Van Allen Probes study of substorm particle injection. *Geophysical Research Letters*, *43*, 6051–6059. https://doi.org/10.1002/2016GL069643

Baker, D. N., Kanekal, S. G., Hoxie, V. C., Batiste, S., Bolton, M., Li, X., Elkington, S. R., et al. (2013). The Relativistic Electron-Proton Telescope (REPT) instrument on board the Radiation Belt Storm Probes (RBSP) spacecraft: Characterization of Earth's radiation belt high-energy particle populations. *Space Science Reviews*, *179*(1-4), 337–381. https://doi.org/10.1007/s11214-012-9950-9

Baker, D. N., Kanekal, S. G., Hoxie, V. C., Henderson, M. G., Li, X., Spence, H. E., Elkington, S. R., et al. (2013). A long-lived relativistic electron storage ring embedded in Earth's outer Van Allen Belt. *Science*, *340*(6129), 186–190. https://doi.org/10.1126/science.1233518

Benacquista, R., Boscher, D., Rochel, S., & Maget, V. (2018). Variations of the electron fluxes in the terrestrial radiation belts due to the impact of corotating interaction regions and interplanetary coronal mass ejections. *Journal of Geophysical Research: Space Physics*, *123*, 1191–1199. https://doi.org/10.1002/2017JA024796

Blake, J. B., Carranza, P. A., Claudepierre, S. G., Clemmons, J. H., Crain, W. R., Dotan, Y., Fennell, J. F., et al. (2013). The Magnetic Electron Ion Spectrometer (MagEIS) instruments aboard the Radiation Belt Storm Probes (RBSP) spacecraft. *Space Science Reviews*, *179*, 383–421. https://doi.org/10.1007/s11214-013-9991-8

Blum, L. W., Bonnell, J. W., Agapitov, O., Paulson, K., & Kletzing, C. (2017). EMIC wave scale size in the inner magnetosphere: Observations from the dual Van Allen Probes. *Geophysical Research Letters*, *44*, 1227–1233. https://doi.org/10.1002/2016GL072316

Blum, L. W., Schiller, Q., Li, X., Millan, R., Halford, A., & Woodger, L. (2013). New conjunctive CubeSat and balloon measurements to quantify rapid energetic electron precipitation. *Geophysical Research Letters*, *40*, 5833–5837. https://doi.org/10.1002/2013GL058546

Borovsky, J. E., Cayton, T. E., Denton, M. H., Belian, R. D., Christensen, R. A., & Ingraham, J. C. (2016). The proton and electron radiation belts at geosynchronous orbit: Statistics and behavior during high-speed stream-driven storms. *Journal of Geophysical Research: Space Physics*, *121*, 5449–5488. https://doi.org/10.1002/2016JA022520

Borovsky, J. E., & Denton, M. H. (2006). Differences between CME-driven storms and CIR-driven storms. *Journal of Geophysical Research*, *111*, A07S08. https://doi.org/10.1029/2005JA011447

Bortnik, J., Chu, X., Ma, Q., Li, W., Zhang, X., Thorne, R. M., Angelopoulos, V., et al. (2018). Artificial neural networks for determining magnetospheric conditions. In E. Comporeale, S. Wing, & J. R. Johnson (Eds.), *Machine Learning Techniques for Space Weather*, (pp. 279–300). Amsterdam, Netherlands: Elsevier Press. https://doi.org/10.1016/B978-0-12-811788-0.00011-1

Claudepierre, S. G., O'Brien, T. P., Blake, J. B., Fennell, J. F., Roeder, J. L., Clemmons, J. H., Looper, M. D., et al. (2015). A background correction algorithm for Van Allen Probes MagEIS electron flux measurements. *Journal of Geophysical Research: Space Physics*, *120*, 5703–5727. https://doi.org/10.1002/2015JA021171

Claudepierre, S. G., O'Brien, T. P., Fennell, J. F., Blake, J. B., Clemmons, J. H., Looper, M. D., Mazur, J. E., et al. (2017). The hidden dynamics of relativistic electrons (0.7–1.5 MeV) in the inner zone and slot region. *Journal of Geophysical Research: Space Physics*, *122*, 3127–3144. https://doi.org/10.1002/2016JA023719

Dessler, A. J., & Karplus, R. (1961). Some effects of diamagnetic ring currents on Van Allen radiation. *Journal of Geophysical Research*, *66*(8), 2289–2295.

Friedel, R. H. W., Reeves, G. D., & Obara, T. (2002). Relativistic electron dynamics in the inner magnetosphere—A review. *Journal of Atmospheric and Solar - Terrestrial Physics*, *64*(2), 265–282. https://doi.org/10.1016/S1364-6826(01)00088-8

Gonzalez, W. D., Joselyn, J. A., Kamide, Y., Kroehl, H. W., Rostoker, G., Tsurutani, B. T., & Vasyliunas, V. M. (1994). What is a geomagnetic storm? *Journal of Geophysical Research*, *99*(A4), 5771. https://doi.org/10.1029/93JA02867

Gonzalez, W. D., Tsurutani, B. T., & Clúa de Gonzalez, A. L. (1999). Interplanetary origin of geomagnetic storms. *Space Science Reviews*, *88*, 529–562.

Hietala, H., Kilpua, E. K. J., Turner, D. L., & Angelopoulos, V. (2014). Depleting effects of ICME-driven sheath regions on the outer electron radiation belt. *Geophysical Research Letters*, *41*, 2258–2265. https://doi.org/10.1002/2014GL059551

Horne, R. B., Lam, M. M., & Green, J. C. (2009). Energetic electron precipitation from the outer radiation belt during geomagnetic storms. *Geophysical Research Letters*, *36*, L19104. https://doi.org/10.1029/2009GL040236

Hudson, M. K., Kress, B. T., Mueller, H.-R., Zastrow, J. A., & Blake, J. B. (2008). Relationship of the Van Allen radiation belts to solar wind drivers. *Journal of Atmospheric and Solar - Terrestrial Physics*, *70*(5), 708–729. https://doi.org/10.1016/jastp.2007.11.003

Hutchinson, J. A., Wright, D. M., & Milan, S. E. (2011). Geomagnetic storms over the last solar cycle: A superposed epoch analysis. *Journal of Geophysical Research*, *116*(A9), A09211. https://doi.org/10.1029/2011JA016463

Kamide, Y., Baumjohann, W., Daglis, I. A., Gonzalez, W. D., Grande, M., Joselyn, J. A., et al. (1998). Current understanding of magnetic storms: Storm-substorm relationships. *Journal of Geophysical Research*, *103*(A8), 17,705–17,728.

Kataoka, R., & Miyoshi, Y. (2006). Flux enhancement of radiation belt electrons during geomagnetic storms driven by coronal mass ejections and corotating interaction regions. *Space Weather*, *4*, S09004. https://doi.org/10.1029/2005SW000211

Katus, R. M., Liemohn, M. W., Gallagher, D. L., Ridley, A., & Zou, S. (2013). Evidence for potential and inductive convection during intense geomagnetic events using normalized superposed epoch analysis. *Journal of Geophysical Research: Space Physics*, *118*, 181–191. https://doi.org/10.1029/2012JA017915

Katus, R. M., M. W. Liemohn, A. J. Ridley, D. L. Gallagher, and S. Zou (2011), Normalized superposed epoch analysis reveals two-step main phase enhancement: Evidence for potential and inductive convection during intense geomagnetic events, Abstract SM41B-2020, 2011 Fall Meeting, AGU, San Francisco, CA, 5–9 Dec.

Kilpua, E. K. J., Balogh, A., von Steiger, R., & Liu, Y. D. (2017). Geoeffective properties of solar transients and stream interaction regions. *Space Science Reviews*, *212*(3-4), 1271–1314. https://doi.org/10.1007/s11214-017-0411-3

Kilpua, E. K. J., Hietala, H., Turner, D. L., Koskinen, H. E. J., Pulkkinen, T. I., Rodriguez, J. V., Reeves, G. D., et al. (2015). Unraveling the drivers of the storm time radiation belt response. *Geophysical Research Letters*, *42*, 3076–3084. https://doi.org/10.1002/2015GL063542

Kilpua, E. K. J., Koskinen, H. E. J., & Pulkkinen, T. I. (2017). Coronal mass ejections and their sheath regions in interplanetary space. *Living Reviews in Solar Physics*, *14*(1), 5. https://doi.org/10.1007/s41116-017-0009-6

Kim, H.-J., Lyons, L., Pinto, V., Wang, C.-P., & Kim, K.-C. (2015). Revisit of relationship between geosynchronous relativistic electron enhancements and magnetic storms. *Geophysical Research Letters*, *42*, 6155–6161. https://doi.org/10.1002/2015GL065192

Lejosne, S., Kunduri, B. S. R., Mozer, F. S., & Turner, D. L. (2018). Energetic electron injections deep in to the inner magnetosphere: A result of the subauroral polarization stream (SAPS) potential drop. *Geophysical Research Letters*, *45*(9), 3811–3819. https://doi.org/10.1029/2018GL077969

Li, W., Thorne, R. M., Bortnik, J., Baker, D. N., Reeves, G. D., Kanekal, S. G., Spence, H. E., et al. (2015). Solar wind conditions leading to efficient radiation belt electron acceleration: A superposed epoch analysis. *Geophysical Research Letters*, *42*, 6906–6915. https://doi.org/10.1002/2015GL065342

Li, X., Baker, D. N., Teremin, M., Cayton, T. E., Reeves, G. D., Selesnick, R. S., Blake, J. B., et al. (1999). Rapid enhancements of relativistic electrons deep in the magnetosphere during the May 15, 1997, magnetic storm. *Journal of Geophysical Research*, *104*(A3), 4467–4476. https://doi.org/10.1029/1998JA900092

Lyons, L. R., & Thorne, R. M. (1973). Equilibrium structure of radiation belt electrons. *Journal of Geophysical Research*, *78*(13), 2142–2149.

Malaspina, D. M., Jaynes, A. N., Boulé, C., Bortnik, J., Thaller, S. A., Ergun, R. E., Kletzing, C. A., et al. (2016). The distribution of plasmaspheric hiss wave power with respect to plasmapause location. *Geophysical Research Letters*, *43*, 7878–7886. https://doi.org/10.1002/2016GL069982

Mann, I. R., Ozeke, L. G., Murphy, K. R., Claudepierre, S. G., Turner, D. L., Baker, D. N., Rae, I. J., et al. (2016). Explaining the dynamics of the ultra-relativistic third Van Allen radiation belt. *Nature Physics*, *12*(10), 978–983. https://doi.org/10.1038/NPHYS3799

Mauk, B. H., Fox, N. J., Kanekal, S. G., Kessel, R. L., Sibeck, D. G., & Ukhorskiy, A. (2013). Science objectives and rationale for the Radiation Belt Storm Probes mission. *Space Science Reviews*, *179*(1-4), 3–27. https://doi.org/10.1007/s11214-012-9908-y

Meredith, N. P., Horne, R. B., Lam, M. M., Denton, M. H., Borovsky, J. E., & Green, J. C. (2011). Energetic electron precipitation during high-speed solar wind stream driven storms. *Journal of Geophysical Research*, *116*(A5), A05223. https://doi.org/10.1029/2010JA016293

Meredith, N. P., Nigel, P., Horne, R. B., Iles, R. H. A., Thorne, R. M., Heynderickx, D., & Anderson, R. R. (2002). Outer zone relativistic electron acceleration associated with substorm-enhanced whistler mode chorus. *Journal of Geophysical Research*, *107*(A7), 1144. https://doi.org/10.1029/2001JA900146

Meredith, N. P., Thorne, R. M., Horne, R. B., Summers, D., Fraser, B. J., & Anderson, R. R. (2003). Statistical analysis of relativistic electron energies for cyclotron resonance with EMIC waves observed on CRRES. *Journal of Geophysical Research*, *108*(A6), 1250. https://doi.org/10.1029/2002JA009700

Millan, R. M., & Thorne, R. M. (2007). Review of radiation belt relativistic electron losses. *Journal of Atmospheric and Solar - Terrestrial Physics*, *69*(3), 362–377. https://doi.org/10.1016/j.jastp.2006.06.019

Miyoshi, Y., Kataoka, R., Kasahara, Y., Kumamoto, A., Nagai, T., & Thomsen, M. F. (2013). High-speed solar wind with southward interplanetary magnetic field causes relativistic electron flux enhancement of the outer radiation belt via enhanced condition of whistler waves. *Geophysical Research Letters*, *40*, 4520–4525. https://doi.org/10.1002/grl.50916

Morley, S. K., Friedel, R. H. W., Spanswick, E. L., Reeves, G. D., Steinberg, J. T., Koller, J., Cayton, T., et al. (2010). Dropouts of the outer electron radiation belt in response to solar wind stream interfaces: Global positioning system observations. *Proceedings of Royal Soceity A*, *466*(2123), 3329–3350. https://doi.org/10.1098/rspa.2010.0078

Moya, P. S., Pinto, V. A., Sibeck, D. G., Kanekal, S. G., & Baker, D. N. (2017). On the effect of geomagnetic storms on relativistic electrons in the outer radiation belt: Van Allen Probes observations. *Journal of Geophysical Research: Space Physics*, *122*, 11,100. https://doi.org/10.1002/2017JA024735–11,108.

Murphy, K. R., Watt, C. E. J., Mann, I. R., Jonathan Rae, I., Sibeck, D. G., Boyd, A. J., Forsyth, C. F., et al. (2018). The global statistical response of the outer radiation belt during geomagnetic storms. *Geophysical Research Letters*, *45*. https://doi.org/10.1002/2017GL076674(9), 3783–3792.

O'Brien, T. P., Lorentzen, K. R., Mann, I. R., Meredith, N. P., Blake, J. B., Fennell, J. F., et al. (2003). Energization of relativistic electrons in the presence of ULF power and MeV microbursts: Evidence for dual ULF and VLF acceleration. *Journal of Geophysical Research*, *108*(A8), 1329. https://doi.org/10.1029/2002JA009784

O'Brien, T. P., McPherron, R. L., Sornette, D., Reeves, G. D., Friedel, R., & Singer, H. J. (2001). Which magnetic storms produce relativistic electrons at geosynchronous orbit? *Journal of Geophysical Research*, *106*(A8), 15,533–15,544.

Pinto, V. A., Kim, H.-J., Lyons, L. R., & Bortnik, J. (2018). Interplanetary parameters leading to relativistic electron enhancement and persistent depletion events at geosynchronous orbit and potential for prediction. *Journal of Geophysical Research: Space Physics*, *123*(2), 1134–1145. https://doi.org/10.1002/2017JA024902.

Reeves, G. D., Baker, D. N., Belian, R. D., Blake, J. B., Cayton, T. E., Fennell, J. F., Friedel, R. H. W., et al. (1998). The global response of relativistic radiation belt electrons to the January 1997 magnetic cloud. *Geophysical Research Letters*, *25*(17), 3265–3268. https://doi.org/10.1029/98GL02509

Reeves, G. D., Friedel, R. H. W., Larsen, B. A., Skoug, R. M., Funsten, H. O., Claudepierre, S. G., Fennell, J. F., et al. (2016). Energy-dependent dynamics of keV to MeV electrons in the inner zone, outer zone, and slot regions. *Journal of Geophysical Research: Space Physics*, *121*, 397–412. https://doi.org/10.1002/2015JA021569

Reeves, G. D., McAdams, K. L., Friedel, R. H. W., & O'Brien, T. P. (2003). Acceleration and loss of relativistic electrons during geomagnetic storms. *Geophysical Research Letters*, *30*(10), 1529. https://doi.org/10.1029/2002GL016513

Reeves, G. D., Spence, H. E., Henderson, M. G., Morley, S. K., Friedel, R. H. W., Funsten, H. O., Baker, D. N., et al. (2013). Electron acceleration in the heart of the Van Allen radiation belts. *Science*, *341*(6149), 991–994. https://doi.org/10.1126/science.1237743

Ripoll, J.-F., Reeves, G. D., Cunningham, G. S., Loridan, V., Denton, M., Santolík, O., Kurth, W. S., et al. (2016). Reproducing the observed energy-dependent structure of Earth's electron radiation belts during storm recovery with an event-specific diffusion model. *Geophysical Research Letters*, *43*, 5616–5625. https://doi.org/10.1002/2016GL068869

Ripoll, J.-F., Santolík, O., Reeves, G. D., Kurth, W. S., Denton, M. H., Loridan, V., Thaller, S. A., et al. (2017). Effects of whistler mode hiss waves in March 2013. *Journal of Geophysical Research: Space Physics*, *122*, 7433–7462. https://doi.org/10.1002/2017JA024139

Shen, X.-C., Hudson, M. K., Jaynes, A., Shi, Q., Tian, A., Claudepierre, S., Qin, M.-R., et al. (2017). Statistical study of the storm time radiation belt evolution during Van Allen Probes era: CME- versus CIR-driven storms. *Journal of Geophysical Research: Space Physics*, *122*, 8327–8339. https://doi.org/10.1002/2017JA024100

Shprits, Y. Y., Kellerman, A., Aseev, N., Drozdov, A. Y., & Michaelis, I. (2017). Multi-MeV electron loss in the heart of the radiation belts. *Geophysical Research Letters*, *44*, 1204–1209. https://doi.org/10.1002/2016GL072258

Shprits, Y. Y., Subbotin, D., Drozdov, A., Usanova, M. E., Kellerman, A., Orlova, K., Baker, D. N., et al. (2013). Unusual stable trapping of the ultrarelativistic electrons in the Van Allen radiation belts. *Nature Physics*, *9*(11), 699–703. https://doi.org/10.1038/NPHYS2760

Spence, H. E., Reeves, G. D., Baker, D. N., Blake, J. B., Bolton, M., Bourdarie, S., Chan, A. A., et al. (2013). Science goals and overview of the Energetic Particle, Composition, and Thermal Plasma (ECT) suite on NASA's Radiation Belt Storm Probes (RBSP) mission. *Space Science Reviews*, *179*(1-4), 311–336. https://doi.org/10.1007/s11214-013-0007-5

Thorne, R. M. (2010). Radiation belt dynamics: The importance of wave-particle interactions. *Geophysical Research Letters*, *37*, L22107. https://doi.org/10.1029/2010GL044990

Thorne, R. M., Li, W., Ni, B., Ma, Q., Bortnik, J., Baker, D. N., Spence, H. E., et al. (2013). Evolution and slow decay of an unusual narrow ring of relativistic electrons near L~3.2 following the September 2012 magnetic storm. *Geophysical Research Letters*, *40*, 3507–3511. https://doi.org/10.1002/grl.50627

Thorne, R. M., Li, W., Ni, B., Ma, Q., Bortnik, J., Chen, L., Baker, D. N., et al. (2013). Rapid acceleration of relativistic radiation belt electrons by magnetospheric chorus. *Nature*, *504*(7480), 411–414. https://doi.org/10.1038/nature12889

Turner, D. L., Angelopoulos, V., Li, W., Hartinger, M. D., Usanova, M., Mann, I. R., Bortnik, J., et al. (2013). On the storm-time evolution of relativistic electron phase space density in Earth's outer radiation belt. *Journal of Geophysical Research: Space Physics*, *118*, 2196–2212. https://doi.org/10.1002/jgra.50151

Turner, D. L., Angelopoulos, V., Morley, S. K., Henderson, M. G., Reeves, G. D., Li, W., Baker, D. N., et al. (2014). On the cause and extent of outer radiation belt losses during the 30 September 2012 dropout event. *Journal of Geophysical Research: Space Physics*, *119*, 1530–1540. https://doi.org/10.1002/2013JA019446

Turner, D. L., Claudepierre, S. G., Fennell, J. F., O'Brien, T. P., Blake, J. B., Lemon, C., Gkioulidou, M., et al. (2015). Energetic electron injections deep into the inner magnetosphere associated with substorm activity. *Geophysical Research Letters*, *42*, 2079–2087. https://doi.org/10.1002/2015GL063225

Turner, D. L., O'Brien, T. P., Fennell, J. F., Claudepierre, S. G., Blake, J. B., Jaynes, A. N., Baker, D. N., et al. (2016). Investigating the source of near-relativistic and relativistic electrons in Earth's inner radiation belt. *Journal of Geophysical Research: Space Physics*, *122*, 695–710. https://doi.org/10.1002/2016JA023600

Turner, D. L., O'Brien, T. P., Fennell, J. F., Claudepierre, S. G., Blake, J. B., Kilpua, E. K. J., & Hietala, H. (2015). The effects of geomagnetic storms on electrons in Earth's radiation belts. *Geophysical Research Letters*, *42*, 9176–9184. https://doi.org/10.1002/2015GL064747

Turner, D. L., Shprits, Y. Y., Hartinger, M. D., & Angelopoulos, V. (2012). Explaining sudden losses of outer radiation belt electrons during geomagnetic storms. *Nature Physics*, *8*(3), 208–212. https://doi.org/10.1038/NPHYS2185

Tverskaya, L. V., Pavlov, N. N., Blake, J. B., Selesnick, R. S., & Fennell, J. F. (2003). Predicting the L-position of the storm-injected relativistic electron belt. *Advances in Space Research*, *31*, 1039–1044.

Ukhorskiy, A. Y., Shprits, Y. Y., Anderson, B. J., Takahashi, K., & Thorne, R. M. (2010). Rapid scattering of radiation belt electrons by storm-time EMIC waves. *Geophysical Research Letters*, *37*, L09101. https://doi.org/10.1029/2010GL042906

Yuan, C. J., & Zong, Q. G. (2013). The double-belt outer radiation belt during CME- and CIR-driven geomagnetic storms. *Journal of Geophysical Research: Space Physics*, *118*, 6291–6301. https://doi.org/10.1002/jgra.50564

Yuan, C. J., & Zong, Q.-G. (2012). Quantitative aspects of variations of 1.5–6.0 MeV electrons in the outer radiation belt during magnetic storms. *Journal of Geophysical Research*, *117*, A11208. https://doi.org/10.1029/2011JA017346

Zhao, H., Baker, D. N., Jaynes, A. N., Li, X., Elkington, S. R., Kanekal, S. G., Spence, H. E., et al. (2017). On the relation between radiation belt electrons and solar wind parameters/geomagnetic indices: Dependence on the first adiabatic invariant and L^*. *Journal of Geophysical Research: Space Physics*, *122*, 1624–1642. https://doi.org/10.1002/2016JA023658

Zhao, H., & Li, X. (2013). Inward shift of outer radiation belt electrons as a function of *Dst* index and the influence of the solar wind on electron injections into the slot region. *Journal of Geophysical Research: Space Physics*, *118*, 756–764. https://doi.org/10.1029/2012JA018179

Zhao, H., Li, X., Baker, D. N., Claudepierre, S. G., Fennell, J. F., Blake, J. B., Larsen, B. A., et al. (2016). Ring current electron dynamics during geomagnetic storms based on the Van Allen Probes measurements. *Journal of Geophysical Research: Space Physics*, *121*, 3333–3346. https://doi.org/10.1002/2016JA022358